Steepest entropy ascent solution for a continuous-time quantum walker

Rohit Kishan Ray [*]

Department of Physics, Indian Institute of Technology Kharagpur, Kharagpur, West Bengal 721302, India

We consider the steepest entropy ascent (SEA) ansatz to describe the nonlinear thermodynamic evolution of a quantum system. Recently this principle has been dubbed the fourth law of thermodynamics [Beretta, Phil. Trans. R. Soc. A **378**, 20190168 (2020)]. A unique global equilibrium state exists in this context, and any other state is driven by the maximum entropy generation principle towards this equilibrium. We study the SEA evolution of a continuous-time quantum walker (CTQW) on a cycle graph with N nodes. SEA solutions are difficult to find analytically. We provide an approximate scheme to find a general single-particle evolution equation governed by the SEA principle, whose solution produces dissipation dynamics. We call this scheme the fixed Lagrange's multiplier (FLM) method. In the Bloch sphere representation, we find trajectories traced out by the Bloch vector within the sphere itself. We have discussed these trajectories under various initial conditions for the case of a qubit. A similar dissipative motion is also observed in the case of CTQW, where probability amplitudes have been used to characterize decoherence. Our FLM scheme shows good agreement with numerical results. As we report, in CTQW, a strong delocalization exists for low system relaxation time.

I. INTRODUCTION

In the era of quantum technologies, quantum algorithms have occupied an important role. Due to the discovery of better-than-classical performance of Shor's algorithm [1] and Grover's search algorithm [2], followed by a plethora of findings, it has become an active area of research to find such algorithms or improve upon existing ones. One such candidate is the quantum analog of the classical random walk, *the quantum walk* [3–12]. Quantum walks are of two kinds, discrete-time quantum walk (DTQW) and continuous-time quantum walk (CTQW) (for a review, see Refs. [13–15] and references therein). Despite having similar probability distributions and features, discrete-time and continuous-time kinds are not equivalent, although, under certain limits, DTQW can produce CTQW [16–18]. In this paper, we focus on CTQW only. Their quadratic speed-up over classical walks characterizes quantum walks (QWs) [14]. QWs have been performed on graphs [19] and can be used to perform a spatial search [4,5]. A scheme for quantum computation has been provided in Ref. [8], where the universality of QWs was explored. Many-body QWs have been studied to understand the nature of entanglement in multipartite systems [10–12,20,21].

Besides studying unitary quantum evolution, many scholars have studied decoherence and dissipation in quantum walks [9,22–26]. Introduction of multicoin walks leads to dissipation [9]. Others have considered decoherence introduced by measurements on the vertices of a graph [25]. Alternatively, some have considered decoherence on the particle, coin, or both [26]. Kendon and Tregenna [25] have shown decoherence to be a useful facet in quantum evolution.

As the walker is an otherwise isolated system, decoherence is introduced as the action of certain measurements on the system in an operational setting [27]. Understanding mixing time under such modeling is an active area of research [28,29]. On the other hand, by using the concept of quantum stochastic walks [30], decoherence in CTQWs has been explored by Garnerone [31] using Lindblad-type master equations. Romanelli [22] split the evolution into two parts, one contributing to the Markovian process, and the other part to the interference responsible for unitary evolution. A novel way of studying thermodynamics has been introduced and followed in Refs. [23,24] by varying the contribution due to the interference factor. Candeloro *et al.* [32] have used quadratic perturbation in the Hamiltonian to study CTQW. However, we are interested in a more fundamental aspect of decoherence—as a first-principle result rather than one of a phenomenological origin. Such a theory should reproduce quantum results under proper limits as desired, besides attempting to explain nonequilibrium behavior.

Studying an open quantum system involves introducing nonunitary behavior in the dynamics. It can be achieved by introducing some superoperators with anticommutation relations invoking dissipation in the system, resulting in a phenomenological origin of the entropy generation process [33]. Consequently, a theory of thermodynamic evolution of quantum states through modeling at different *levels of description* to arrive at the equation of motion has been in vogue [34,35]. Theories belonging to this category can be classified as a general equation for the nonequilibrium reversible-irreversible coupling (GENERIC). In this setup, microscopic details of the fundamental structure are ignored in favor of macroscopic dynamics. As a consequence, the constraints become global invariants of motion. The GENERIC theory essentially lacks a local description, which can be modeled using

*rohitkray@iitkgp.ac.in

a metric-dependent relaxation parameter [36], and a concept of equilibrium to drive the system. Let us consider global and local equilibriums in the Lyapunov sense [37]. We find an evolution trajectory in the state space characterized by maximization of the entropy production rate under the constraint of invariants of the motion [38–48]. In addition to this, consider the second law of thermodynamics: the existence of a unique globally stable state to satisfy the second law requirement [49]. (A rich review of literature in this domain is compiled in the Ref. [50].) The unitary trajectories described by Schrödinger-type evolution form limit cycles in this notion [51]. As a result, states that belong to the quantum mechanical evolution are extrema of the set containing all such states considered in the description. This description also requires the identification of the density matrix as a valid state operator and $\rho^2 = \rho$ to be the defining feature of pure QM limit cycles. In the case of a qubit, the rest of the $\text{tr}(\rho^2) \leqslant 1$ states thus fill up the entire Bloch sphere and represent the state space available for nonlinear evolution.

The steepest entropy ascent (SEA) dynamics framework finds its roots in the first-principle approach to understand "spontaneous decoherence." Moreover, the SEA formalism can be extended to other disciplines of studying nonlinear evolution of a more general kind [52]. In follow-up work, under similar kinematic considerations, the mathematical equivalence between the nonlinear contribution due to GENERIC and SEA has been drawn by Montefusco *et al.* [53]. While working in a far-off equilibrium situation, defining temperature becomes troublesome, as the temperature is defined using steady states. The concept of hypoequilibrium as invoked in Refs. [54,55] seems to serve this purpose. In this SEA theory, we wish to solve for the continuous-time quantum walker and analyze the solution.

In a nutshell, quantum walks can be useful with decoherence. This decoherence is usually modeled through measurements performed at each walk instance, and the walker state mixes according to some rule. However, when a first-principle approach (SEA-type dynamics) involving a local description and an entropy nondecrease postulate is considered to study the relaxation of a system subject to initial perturbation, decoherence results without external interaction. We consider a single quantum walker walking on a cycle of N nodes in continuous time, whose evolution is guided by the SEA formalism. Its solution can be applied to any time-independent Hamiltonian containing a single particle. We show that the time-dependent relaxation dynamics characterize this evolution. Under such a scenario, both SEA and unitary dynamics can be recovered. Section II introduces the readers to preliminary physical ideas. Here we discuss the basics of the continuous-time quantum walk and the building blocks of the SEA principle to keep the paper self-contained. In Sec. III we first derive an approximate analytical solution. As the SEA equation of motion (EoM) [Eq. (8) below] is highly nonlinear, it is difficult to solve analytically [43,46], and we resort to numerical solutions. This limits our ability to understand the dynamics analytically. Interestingly, though, as shown in Sec. III A, considering a fixed Lagrange's multiplier (FLM) approach eases the inherent nonlinearity of the EoM, making the solution analytically tractable. As an application of this, we solve for a two-level system: a qubit, which closely

agrees with the exact result [43] present in the literature. In the second part of Sec. III, we solve for the N-level system—a quantum walker and show plots of the solutions followed by our analysis. We have delegated detailed derivations to the Appendixes to preserve the flow of this paper. In some cases, the readers are requested to go through the references provided. In Sec. IV we discuss the importance of our result and conclude by pondering further questions that have come up through this work. The Appendixes are structured as follows: in Appendix A we have provided the geometric interpretation of SEA evolution. We have shown how the SEA EoM is derived using the variational principle. In the following Appendix B, we derive the expressions for Lagrange multipliers and provide the complete SEA equation of motion. Appendix C contains comments on relaxation time, and in Appendix D we have computed the Lagrange multipliers for the CTQW.

II. THEORETICAL PRELIMINARIES

Consider a quantum walker walking on some undirected graph $\mathcal{G}$ with N vertices, vertex, and edge set as $\mathbb{V}$ and $\mathbb{E}$, respectively. $\mathcal{G}$ has no double edge or self-loops. The adjacency matrix $\mathbf{A}$ of $\mathcal{G}$ can be defined as follows:

$$\mathbf{A} : a_{ij} = \begin{cases} 1 & \text{if } e_{ij} \in \mathbb{E} \\ 0 & \text{otherwise.} \end{cases}$$

Thereafter, we can define the Laplacian $\mathbf{L}$ of $\mathcal{G}$ as [4,56]

$$\mathbf{L} = \mathbf{D} - \mathbf{A},$$

where $\mathbf{D}$ is diagonal and has an entry as the degree of the ith vertex, d_i. We associate a hopping probability μ_{ij} with the probability of transition between two adjacent vertices (v_i, v_j) per unit time. Considering uniform transition rates $\mu_{ij} = \mu$, for the unitary continuous-time quantum walker we can write [4,13,25]

$$\frac{d|\Psi\rangle}{dt} = -\frac{i}{\hbar}\mu\mathbf{L}|\Psi\rangle. \tag{1}$$

In Eq. (1), the quantity $\mu\mathbf{L}$ is identified as the Hamiltonian $\mathcal{H}$ of the CTQW. The solution to Eq. (1) is read as

$$|\Psi(t)\rangle = \exp(-i\mu\mathbf{L}t)|\Psi(0)\rangle \equiv \mathcal{U}(t)|\Psi(0)\rangle \equiv \mathcal{U}_t|\Psi(0)\rangle, \tag{2}$$

where $|\Psi(0)\rangle$ is the initial state of the walk, and $\hbar = 1$. In terms of density matrix ρ,[1] we can write Eq. (2) as

$$\rho^t = \mathcal{U}_t \rho^0 \mathcal{U}_t^\dagger, \tag{3}$$

implying that the quantum state of the walker undergoes unitary rotation in the state space as the walker exhibits CTQW.

Steepest entropy ascent motion concerns about the relaxation of a system away from equilibrium. The interested readers are directed towards Refs. [49,52,54,57] for a detailed understanding of SEA dynamics. Here we explore the observed results while delegating a basic introduction to Appendix A, where the derivation of the SEA EoM is done in

---

[1]t is added to the superscript as a label for a time, instead of using the standard $\rho(t)$, to make the notations less cumbersome.

brief. In the SEA evolution, the dynamical equation can be written in the general Ginzburg-Landau form [54] as under

$$\frac{d\rho}{dt} = -i[\mathcal{H}, \rho] + \frac{1}{\tau}\{\mathcal{D}, \rho\}, \qquad (4)$$

where $\{\cdot, \cdot\}$ represents anticommutator, τ relaxation time, and $\mathcal{D}$ is related to dissipation, the nonunitary part of the evolution. In the SEA formalism, the state operator $\gamma \equiv |\gamma\rangle$ is an element of linear manifold $\mathcal{L}$, a state space in Hilbert space $\mathcal{H}$, with a symmetric inner product $(A \mid B) = \text{Tr}(A^\dagger B + B^\dagger A)/2$ [52]. To maintain a positive ρ for all times of SEA motion, the square root of ρ is considered the state operator and is computed using a spectral theorem [36], $\rho = \gamma\gamma^\dagger$. Let the set $\{\mathbf{C_i}(\gamma)\}$ contain operators denoting various conservation quantities to be used as constraints of motion, such as energy ($\mathcal{H}$), number of particles ($\mathcal{N}$), etc. The functional derivative of $\mathbf{C_i}$ is denoted by $|\Psi_i\rangle = |\delta\mathbf{C_i}(\gamma)/\delta\gamma\rangle$. Similarly, the entropy functional is ($k \equiv k_B$, Boltzmann's constant)

$$\mathbf{S} = -k\text{Tr}[\rho\ln(\rho)],$$

and its functional derivative is $|\Phi\rangle = |\delta\mathbf{S}(\gamma)/\delta\gamma\rangle$ [52,57]. The constraint of entropy nondecrease and conservation of $\mathbf{C_i}$ can be expressed as

$$\frac{d\mathbf{S}}{dt} = \Pi_S \quad \text{with} \quad \Pi_S = (\Phi \mid \Pi_\gamma) \geqslant 0, \qquad (5)$$

$$\frac{d\mathbf{C_i}}{dt} = \Pi_{C_i} \quad \text{with} \quad \Pi_{C_i} = (\Psi_i \mid \Pi_\gamma) = 0. \qquad (6)$$

Using the above constraint equation, and by applying Lagrange's multiplier method, the SEA rate of change of state operator, $\frac{d\gamma}{dt} = \Pi_\gamma$ is given as

$$|\Pi_\gamma) = \mathcal{L}\left|\Phi - \sum_i \beta_i\Psi_i\right), \qquad (7)$$

where the metric associated with the manifold $\mathcal{L}$, $\hat{G}(\gamma)$ appears as $\mathcal{L} = \frac{1}{\tau}\hat{G}(\gamma)^{-1}$ [52]. This can be rewritten in terms of ρ (see Appendix A for details) for a uniform (Fisher) metric as

$$\frac{d\rho}{dt} = -\frac{1}{\tau}\left[\rho\ln(\rho) + \frac{1}{2}\sum_i(-1)^i\beta_i\{\mathbf{C_i}, \rho\}\right] - i[\mathcal{H}, \rho]. \qquad (8)$$

Comparing with Eq. (4), we can write $\{\mathcal{D}, \rho\} = -[k\rho\ln(\rho) + \frac{1}{2}\sum_i(-1)^i\beta_i\{\mathbf{C_i}, \rho\}]$. Choosing τ, β_i as Lagrange's multipliers, the full SEA evolution, including the expressions for the β_i's, can be written in the following compact form conveying all the necessary information (see Appendix B):

$$\frac{d\rho}{dt} + i[\mathcal{H}, \rho] = -\frac{1}{\tau}\frac{\begin{vmatrix} \rho\ln(\rho) & \frac{1}{2}\{\mathbf{C_1}, \rho\} & \frac{1}{2}\{\mathbf{C_2}, \rho\} & \frac{1}{2}\{\mathbf{C_3}, \rho\} \\ \text{tr}(\frac{\rho}{2}\{\mathbf{C_1}, \ln(\rho)\}) & \text{tr}(\rho\mathbf{C_1}^2) & \text{tr}(\frac{\rho}{2}\{\mathbf{C_1}, \mathbf{C_2}\}) & \text{tr}(\frac{\rho}{2}\{\mathbf{C_1}, \mathbf{C_3}\}) \\ \text{tr}(\frac{\rho}{2}\{\mathbf{C_2}, \ln(\rho)\}) & \text{tr}(\frac{\rho}{2}\{\mathbf{C_2}, \mathbf{C_1}\}) & \text{tr}(\rho\mathbf{C_2}^2) & \text{tr}(\frac{\rho}{2}\{\mathbf{C_2}, \mathbf{C_3}\}) \\ \text{tr}(\frac{\rho}{2}\{\mathbf{C_3}, \ln(\rho)\}) & \text{tr}(\frac{\rho}{2}\{\mathbf{C_3}, \mathbf{C_1}\}) & \text{tr}(\frac{\rho}{2}\{\mathbf{C_3}, \mathbf{C_2}\}) & \text{tr}(\rho\mathbf{C_3}^2) \end{vmatrix}}{\begin{vmatrix} \text{tr}(\frac{\rho}{2}\{\mathbf{C_1}, \mathbf{C_1}\}) & \text{tr}(\frac{\rho}{2}\{\mathbf{C_1}, \mathbf{C_2}\}) & \text{tr}(\frac{\rho}{2}\{\mathbf{C_1}, \mathbf{C_3}\}) \\ \text{tr}(\frac{\rho}{2}\{\mathbf{C_2}, \mathbf{C_1}\}) & \text{tr}(\frac{\rho}{2}\{\mathbf{C_2}, \mathbf{C_2}\}) & \text{tr}(\frac{\rho}{2}\{\mathbf{C_2}, \mathbf{C_3}\}) \\ \text{tr}(\frac{\rho}{2}\{\mathbf{C_3}, \mathbf{C_1}\}) & \text{tr}(\frac{\rho}{2}\{\mathbf{C_3}, \mathbf{C_2}\}) & \text{tr}(\frac{\rho}{2}\{\mathbf{C_3}, \mathbf{C_3}\}) \end{vmatrix}}. \qquad (9)$$

To solve for CTQW, we identify $\mathbf{C_2}$ with $\mu\mathbf{L}$, and use probability conservation ($\mathbf{C_1} = \mathbf{I}$). We do not need $\mathbf{C_3}$ for a single walker; the number operator becomes redundant. Thence,

$$\mathcal{D} = -[k\ln(\rho) - \beta_I\mathbf{I} + \beta_H\mu\mathbf{L}]. \qquad (10)$$

Substituting this expression for $\mathcal{D}$ in Eq. (4), we solve for ρ. Interestingly, we note that Eq. (8) is free of γ, making it a deterministic process [51].

III. APPROXIMATE ANALYTICAL SOLUTIONS OF THE FULL SEA EVOLUTION

A. Single-particle case (arbitrary dimension)

In this section, we solve Eq. (8) for a single particle in arbitrary dimensions under a given Hamiltonian $\mathcal{H}$. The motion is constrained by the condition of entropy $\mathbf{S}$ nondecrease, along with conservation of quantities $\mathbf{C_i}$ such as energy, probability, etc. These conditions are introduced via Lagrange multipliers β_i's in Eq. (8). These β_i are nontrivially dependent on ρ, which makes it difficult to solve Eq. (9) analytically with such nonlinearity; therefore, we resort to numerical techniques.

However, an approximate analytical solution can help us understand the essence of the general nonlinear evolution.

In this work we introduce the following approximation. We consider the β_i's [defined in Eq. (B2)] to be at their prefixed values, such as their initial or final values, and call this approximation the fixed Lagrange's multiplier (FLM) method.[2] The FLM method enables us to have an approximate analytic expression for the single quantum constituent case, which produces results in good agreement with the numerical computation. We begin with a general ρ. Since ρ is always positive, such a ρ can have a diagonalization which can be achieved via a similarity transformation, a trace-preserving operation. Let us consider one such a transformation on a

---

[2]There is a natural motivation behind this assumption. Consider a real function $f(x, y)|x, y \in \mathbb{R}$, to be optimized under some constraint $g(x, y) = c$, where c is a real constant. We can define a *Lagrangian* function $L(x, y, c) := f(x, y) + \lambda[c - g(x, y)]$ with $\lambda = \frac{\partial L}{\partial c}$ as the Lagrange's multiplier. This suggests, for a fixed c, that there exists a constant λ such that $f(x, y)$ is optimized.

given ρ as follows:

$$\rho^t = \mathbf{U}_t \rho_d^t \mathbf{U}_t^{-1},$$

where $\mathbf{U}_t$ is formed by columnwise stacking the eigenvectors of ρ at time t, and ρ_d^t is the required diagonal matrix. Using this transformation in Eq. (8) we get

$$\frac{d\rho_d^t}{dt} = -\frac{1}{2\tau} \left[\{\ln(\rho_d^t), \rho_d^t\} + \sum_i (-1)^i \beta_i \{\mathbf{C_i}^d, \rho_d^t\} \right] - i[\mathcal{H}^d, \rho_d^t]. \tag{11}$$

Note that $\mathcal{H}^d = \mathbf{U}_t^{-1}\mathcal{H}\mathbf{U}_t$ and $\mathbf{C_i}^d = \mathbf{U}_t^{-1}\mathbf{C_i}\mathbf{U}_t$.[3]

Before we proceed, certain comments are necessary. First, we note $\frac{d\rho^t}{dt} = [\dot{\mathbf{U}}_t\mathbf{U}_t^{-1}, \rho^t] + \mathbf{U}_t\dot{\rho}_d^t\mathbf{U}_t^{-1}$, thus implying, in general, eigenvectors can have nonzero time dependence. However, a restricted class of problems exists, where the eigenbasis of ρ can change solely due to the Hamiltonian. In such a scenario, the commutator term appearing in the time derivative becomes zero, and we are left with constant $\mathbf{U}_t$. As a result, we have a special class of evolution where a ρ initially diagonal in energy basis remains so throughout the dynamics. In the subsequent computations, we exploit this "diagonal property" of ρ to find an analytic approximation. Although this limits the range of evolutions considerable under the given assumption, it still pertains to a broad class of solutions as supported by the examples presented in the paper.

ρ has a spectral decomposition in its eigenbasis $\{|\lambda_i\rangle\}$, and ρ_d is diagonal in the standard basis $\{|i\rangle\}$ ($|i\rangle$ is an N-dimensional unit vector) as follows:

$$\rho_d = \sum_{ij} \lambda_i \delta_{ij} |i\rangle\langle j| \quad \text{and} \quad \begin{aligned} \rho &= \sum_i \lambda_i |\lambda_i\rangle\langle\lambda_i|, \\ &= \sum_{ij} \lambda_i \delta_{ij} |\lambda_i\rangle\langle\lambda_j|, \end{aligned}$$

where δ_{ij} is the Kronecker delta. Using these expansions in Eq. (11), and by choosing $[\mathcal{H}^d]_{ij} = H_{ij}^d$, and $[\mathbf{C_s}^d]_{ij} = C_{ij}^s$, the r.h.s. of Eq. (11) can be modified as

$$-\frac{1}{2\tau} \sum_{ijm} \delta_{im} \left[2\lambda_m \ln(\lambda_m)\delta_{mj} \right.$$

$$+ \sum_s (-1)^s \beta_s [\lambda_m + \lambda_j] C_{mj}^s \bigg] |i\rangle\langle j|$$

$$- i \sum_{ij} [\lambda_j - \lambda_i] H_{ij}^d |i\rangle\langle j|.$$

For a single particle, we are mostly interested in energy and probability conservation; the complete expression upon

considering a Euclidean metric reads as

$$\sum_{ij} \dot{\lambda}_i \delta_{ij} |i\rangle\langle j| = -i \sum_{ij} (\lambda_j - \lambda_i) H_{ij}^d |i\rangle\langle j|$$

$$-\frac{1}{2\tau} \sum_{ij} \left[2k\lambda_i \ln(\lambda_i)\delta_{ij} - 2\beta_I \lambda_i \delta_{ij} \right.$$

$$+ \beta_H(\lambda_j + \lambda_i) H_{ij}^d \bigg] |i\rangle\langle j|.$$

According to our assumption the l.h.s. of Eq. (11) is diagonal:

$$\frac{d\lambda_i}{dt} = -\frac{1}{\tau} \left[\lambda_i \ln(\lambda_i) - \beta_I \lambda_i + \beta_H \lambda_i H_{ii}^d \right]. \tag{12}$$

For diagonal density matrices, similarity transformation is identity, so we get

$$\frac{dp_i}{dt} = -\frac{1}{\tau}[p_i \ln(p_i) - \beta_I p_i + \beta_H p_i H_{ii}], \tag{13}$$

where $p_i = [\rho^t]_{ii}$. Both Eqs. (12) and (13) have a similar type of solution, namely, that of almost identical nonlinear ODE. Using standard techniques and FLM approximation, we arrive at the following expression:

$$p_i(t) = \exp\left[\exp\left(w_i - \frac{t}{\tau}\right) + \beta_I - \beta_H H_{ii} \right]. \tag{14}$$

We have $w_i = \ln[\ln(p_i^0) - \beta_I + \beta_H H_{ii}]$, where p_i^0 is the ith diagonal entry of initial ρ. The solution produced above can be written in a straightforward form, identifying $\eta_i^c = \beta_H H_{ii} - \beta_I$, or for general cases as $\sum_s (-1)^s \beta_s C_{ii}^s$, $\tilde{v}_i = e^{w_i}$, and $\eta(t) \equiv \eta^t = \exp(-t/\tau)$, we get

$$p_i(t) \equiv p_i^t = \exp\left(\tilde{v}_i \eta^t - \eta_i^c\right). \tag{15}$$

We find $\tilde{v}_i$ as

$$p_i(0) = p_i^0,$$

$$\exp(\tilde{v}_i \eta^0 - \eta_i^c) = p_i^0,$$

$$\Rightarrow \tilde{v}_i = \ln\left(p_i^0\right) + \eta_i^c.$$

Hence, we can write $\rho_d^t = \sum_i p_i^t |i\rangle\langle i|$. A general initial ρ with off-diagonal terms can be written as $\rho = \mathbf{U}_t \rho_d^t \mathbf{U}_t^{-1}$, whereas if we consider only diagonal ρ's, we get $\rho = \rho_d^t$. Including the Hamiltonian evolution, we get the following equation for uniform metric ($\mathcal{U}_t \equiv \exp(-i\mathcal{H}t)$, and projections $\mathbb{P}_m = |m\rangle\langle m|$):

$$\rho^t = \mathcal{U}_t \mathbf{U}_t \left(\sum_m \exp\left(\eta_m^t - \eta_m^c\right) \mathbb{P}_m \right) \mathbf{U}_t^{-1} \mathcal{U}_t^\dagger, \tag{16}$$

where $\eta_m^t = (\ln(p_m^0) + \eta_m^c)e^{-t/\tau} = \tilde{v}_m \eta^t$ and $\eta_m^c = \sum_s (-1)^s \beta_s C_{mm}^s$. So far, as we can see, Eq. (16) represents the evolution of ρ^t's diagonal in the energy basis, except that it considers only the Fisher metric. We use this equation to understand spontaneous decoherence in the evolution of a walker performing CTQW [see Eqs. (1)–(3)]. We consider the case of a two-level system and use Eq. (16) to observe its motion on the Bloch sphere. Despite the problem's simplicity, it is a sparsely explored area even within the community [43,49]. A qubit evolution can help us understand some of the salient features of SEA dynamics. In this spirit, and for the sake of consistency in presentation, we explore the two-level

---

[3]Note that neither $\mathcal{H}^d$ nor $\mathbf{C_i}^d$ is the diagonal form of the respective matrices (they could be, if they can be simultaneously diagonalized with ρ). I was running out of symbols; any confusion due to this is regretted.
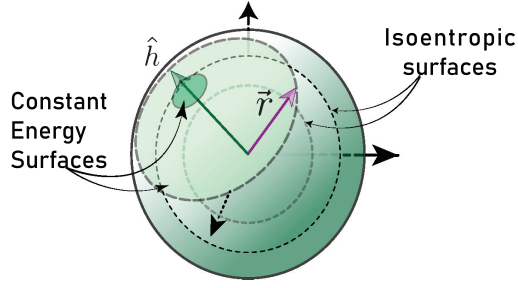
FIG. 1. A Bloch sphere representation of a qubit. The purple arrow denotes the vector $\vec{r}$, and the green one $\hat{h}$. The isoentropic concentric surfaces and the constant energy planes are labeled in the diagram.

system in detail to appreciate the results for the N-level system with relative ease.

B. Case I: Two-level system: Qubit

A general two-level quantum system can be represented by a qubit with two possible outcomes of a measurement, i.e., level 1, $|0\rangle$, and level 2, $|1\rangle$. The most general density matrix representing a qubit can be expressed in the following form:

$$\rho = \frac{1}{2}(I + \vec{r} \cdot \vec{\sigma}),$$

where $\vec{\sigma}$ is the Pauli vector with components as Pauli matrices for a spin-$\frac{1}{2}$ system, and $\vec{r}$ is the radial vector of a Riemann sphere, also known as a Bloch sphere [27].

The most general Hamiltonian acting on a point on this sphere can be written as $\mathcal{H} = (\omega_0 I + \omega \hat{h} \cdot \vec{\sigma})$, where $\hat{h}$ is a unit vector along the axis of rotation due to $\mathcal{H}$, and $\hbar = 1$. Eigenvalues of $\mathcal{H}$ are $h_\pm = \omega_0 \pm \omega$, $h = |\hat{h}| = 1$, and 2ω is the precession frequency of the state vector around $\hat{h}$, ω_0 is a constant $= \frac{1}{2}\mathrm{tr}(\mathcal{H})$ [43]. Figure 1 shows that the states are constrained to lie on the intersection of constant energy and isoentropic surfaces. The figure shows that on each isoentropic surface, the radius vector traces out the intersection of constant energy planes (perpendicular to $\hat{h}$) with the surface.

We notice that to include mixed states in our description, $\vec{r}$ has variable magnitude r^t, and the maximally mixed state is represented by $\vec{r} = \vec{0}$. Considering $\mathrm{tr}(\rho^2) = R$, eigenvalues of ρ, $\lambda_\pm = \frac{1}{2}(1 \pm r)$, we can see immediately

$$r = \sqrt{2R - 1},$$

which further implies $0 \leqslant r \leqslant 1$, for $\frac{1}{2} \leqslant R \leqslant 1$.

Using the eigenvalues $\lambda_\pm$ we can write the entropy function as

$$\begin{aligned}
\mathbf{S} &= -k[\lambda_+ \ln(\lambda_+) + \lambda_- \ln(\lambda_-)] \\
&= -k\left[\frac{1+r}{2}\ln\left(\frac{1+r}{2}\right) + \frac{1-r}{2}\ln\left(\frac{1-r}{2}\right)\right] \\
&= -\frac{k}{2}\ln\left(\frac{1-r^2}{4}\right) - \frac{kr}{2}\ln\left(\frac{1+r}{1-r}\right).
\end{aligned} \quad (17)$$

The isoentropic surfaces form concentric spheres, with entropy increasing as r decreases. Therefore, the main dissipative part of the dynamics will try to draw any state within and

on the surface of the Bloch sphere toward its center, where a maximally mixed state with maximum entropy $k \ln(2)$ resides. Since pure unitary dynamics is nondissipative, it is required and customary to initially disturb (quench) a quantum mechanical state from the limit cycle of unitary evolution and then observe the system's relaxation as time progresses. The maximally mixed state is the global equilibrium (ρ_u) state for a completely isolated system. Thus, we quench the initial state (ρ^0) as follows [48]:

$$\rho = \varepsilon \rho^0 + (1-\varepsilon)\rho_u,$$

$$\sum_i \lambda_i |\lambda_i\rangle\langle\lambda_i| = \sum_i \varepsilon\lambda_i^0 |\lambda_i^0\rangle\langle\lambda_i^0| + (1-\varepsilon)\frac{I}{\mathrm{tr}(I)}.$$

If ρ^0 is diagonal, then

$$\lambda_i' = \varepsilon\lambda_i^0 + (1-\varepsilon)\frac{1}{N}, \quad (18)$$

where $N = \mathrm{tr}(I)$, which for this case is 2. ε is a variable parameter $\in [0, 1]$, with zero value denoting the completely mixed state. Armed with all these and a Euclidean metric, we consider Eq. (12):

$$\frac{d\lambda_\pm}{dt} = -\frac{1}{\tau}\left[\lambda_\pm \ln(\lambda_\pm) + (\beta_H H_\pm^d - \beta_I)\lambda_\pm\right]$$

$$\Rightarrow \pm\dot{r} = \mp\frac{1}{\tau}\left[(1 \pm r)\ln\left(\frac{1 \pm r}{2}\right) + (\beta_H H_\pm - \beta_I)(1 \pm r)\right].$$

After that, we can write for the dissipative part of the motion as before:

$$r^t = -1 + 2\exp[(\eta_+^t - \eta_+^c)], \text{ for } \lambda_+, \text{ and}$$

$$r^t = 1 - 2\exp[(\eta_-^t - \eta_-^c)], \text{ for } \lambda_-.$$

Thence,

$$r^t = [\exp(\eta_+^t - \eta_+^c) - \exp(\eta_-^t - \eta_-^c)], \quad (19)$$

and

$$\Rightarrow \lambda_\pm(t) = \exp(\eta_\pm^t - \eta_\pm^c),$$

where $\eta_\pm^t = [\ln(\lambda_\pm') + (\beta_H H_\pm - \beta_I)]e^{-\frac{t}{\tau}}$, λ' as in Eq. (18). The full evolution is given by

$$\mathcal{U}_t \mathbf{diag}[\exp(\eta_+^t - \eta_+^c), \exp(\eta_-^t - \eta_-^c)]\mathcal{U}_t^\dagger. \quad (20)$$

This solution above in Eq. (20) works when we have Lagrange multipliers determined using prefixed conditions, i.e., the FLM method. Otherwise, in general β_i's depend on time-dependent r and on constant $r_e = \hat{h} \cdot \vec{r}$. Consequently, Eq. (19) needs to be solved numerically. For a detailed analysis, start from the differential equation given in Appendix B, Eq. (B15).

Let us now understand the SEA approach through simple well-known, and well-studied physical conditions. We take $\hat{h} = \hat{z}$, and focus on the states lying on the equatorial plane of the Bloch sphere, $r_e = 0$. $\mathcal{H}$ in this scenario becomes $\omega\sigma_z$, which is diagonal in the standard basis. Using the expression for λ' provided in Eq. (18), we write the β_i's as [Eqs. (B16)
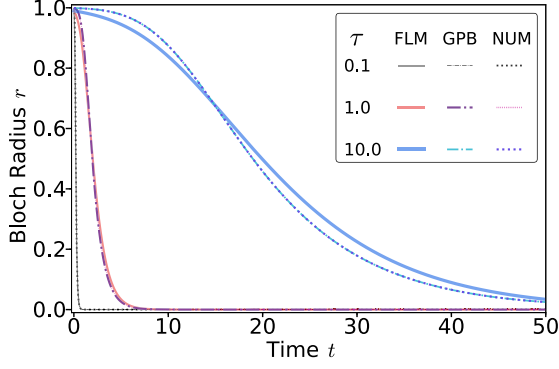
FIG. 2. Plot of the radial distance of the state operator in the Bloch sphere over time ($t = 50$) for a qubit under various τ (first column of the legend), with $\omega = 5$, and $\varepsilon = 0.999$. As discussed in the paper, the higher τ states fall slowly compared to lower valued ones. Solid lines represent computation done using FLM, dot-dash lines GPB are plotted using Eq. (23) [43], and the dotted NUM lines are plotted using direct numerical simulation of Eq. (8).

and (B17)]

$$\beta_H = 0,$$
$$\beta_I = \frac{k}{2}\left[\ln\left(\frac{1-\varepsilon^2}{4}\right) + \varepsilon \ln\left(\frac{1+\varepsilon}{1-\varepsilon}\right)\right]. \quad (21)$$

Let the initial ρ be $a|0\rangle\langle 0| + b|1\rangle\langle 1|$. Then radius r' after quenching is $r' = \varepsilon r = \varepsilon|a - b|$. We get $\eta_\pm^t = [\ln(\frac{1\pm\varepsilon}{2}) - \beta_I]e^{-\frac{t}{\tau}}$, and $\eta_\pm^c = \beta_I$. Finally, the evolution equation becomes

$$r^t = (e^{\theta_+^t} - e^{\theta_-^t}), \quad (22)$$

where $\theta_\pm^t = \eta_\pm^t - \eta_c\pm$. For $\omega = 5$ and $\varepsilon = 0.999$,[4] we graphically show the evolution of r^t in Fig. 2. As evident from the form of the general dynamical equation (4), τ acts as a modulating factor, where high τ results in a smaller dissipation contribution. Trivial mathematical interpretations aside, system relaxation time τ behavior is inversely related to the entropy production rate. After the system goes through a quenching process, it relaxes and could either thermalize or localize. This behavior is dependent mainly on the speed at which this happens. Higher τ implies slower relaxation, while as noted in literature, lower positive values of τ result in the steepest ascent of entropy, as we see in Fig. 3. In the expression of η_t [Eq. (14)], the exponent has $(\frac{-t}{\tau})$ dependence, which implies in $\frac{t}{\tau} \ll 1$ we will have a nondissipative feature, and at $\frac{t}{\tau} \sim 1$ we will have the desired dissipation.
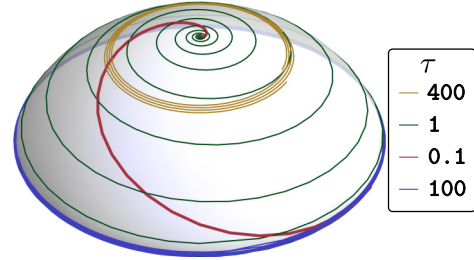
From Fig. 2 we see higher τ-valued states will have more delayed and gradual relaxation. To corroborate our results with the existing ones in the literature, we consult the solution provided in Ref. [43, Eq. (19)] (GPB), reproduced below:

$$r^t = \tanh\left[\frac{1}{2}\exp\left(-\frac{t}{\tau}\right)\ln\left(\frac{1+\varepsilon}{1-\varepsilon}\right)\right]. \quad (23)$$

Finally, we have plotted the numerical solution (NUM) of Eq. (8). We can see that the GPB solution matches the
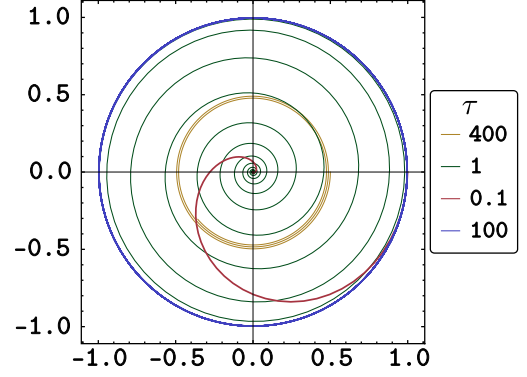
FIG. 3. (a) The spiraling trajectory of the state operator in the equatorial plane of the Bloch sphere, as viewed from its north pole after $t = 30$. Different τ values show the difference between each trajectory. (b) Evolution of states after $t = 30$, on the surface of revolution generated from the entropy functional expression. The legend identifies the τ values considered for this plot. The case with $\tau = 400$ corresponds to the case with $\varepsilon = 0.5$, while the rest of the cases have $\varepsilon = 0.999$. Lower τ states rise faster, and the lowest has the steepest ascent.

NUM results. FLM values, on the other hand, lie somewhat close, yet the initial and final agreements between FLM and GPB/NUM are intriguing, given that FLM is an approximation. Depending on the β_i considered, FLM can be fine-tuned. If we fix β_i at initial values, FLM better represents far-from-equilibrium behavior and equilibrium behavior (Fig. 2). However, FLM tuned using the final value of β_i does a better job representing the near-equilibrium feature but does not fare equally well in the far-from-equilibrium region. Moreover, as τ changes, disagreement between the FLM and GPB/NUM increases.

We show the spiraling motion to the center of the Bloch sphere on the equatorial plane in Fig. 3(a). Here we see that high τ states remain near the pure states for a longer time than low-valued ones, as they almost instantaneously mix to the maximum entropic state. These low values of τ trajectories represent the steepest entropy ascent solution. This steep *ascent* can be better visualized when we consider the surface of revolution generated from the entropy functional in Eq. (17) and plot these spiral trajectories onto that surface as shown in Fig. 3(b). We see that with time each trajectory tries to rise to the top of the surface where the point with maximum entropy is present. We can also see that high τ states maintain
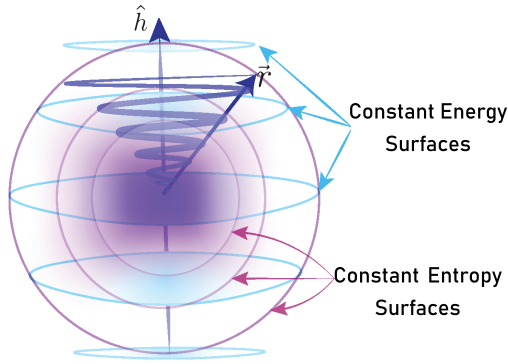
FIG. 4. A schematic depiction of a qubit state's general energy dissipative evolution (purple spiral in the online colored version). This schematic is for high τ values; for low values of the same, the trajectory will follow a straighter path, as indicated in Ref. [58], which will also be the steepest ascent.

a limiting behavior at the foot of the surface of revolution, taking almost forever to reach the top (unitary-type behavior). A schematic evolution of the general nonenergy-conserving motion for a qubit under SEA is presented in Fig. 4. As energy continues decreasing, the value of r_e also decreases. The state arrives at the global equilibrium when it reaches zero at the center. Next, we consider the evolution of a walker performing a continuous-time quantum walk under spontaneous decoherence.

C. Case II: N-level system: Quantum walker

As done in the previous subsection, we can very well use a Bloch vector representation for a $d = N$-dimensional qudit state space as a $\mathbb{R}^{N^2-1}$ dimensional ball [59–63], with a unit vector $\vec{r}$ associated with the space. We write ρ as [63]

$$\rho = \frac{1}{N}\left(\mathrm{I} + \sqrt{\frac{N(N-1)}{2}}\vec{r}\cdot\vec{\Gamma}\right), \quad (24)$$

where $\vec{\Gamma}$ is a Pauli-type generalization in N dimension, comprising generators of SU(N) along with the identity operator I [61]. Yet this is not a trivial generalization of the familiar Bloch sphere representation because in dimensions $N \geqslant 3$, the expression (24) does not offer a bijective mapping like the qubit case. In the qubit scenario, each point on and inside the Bloch sphere has a one-to-one correspondence with a physical state, referring to a semipositive density matrix with unit trace. We sometimes get nonphysical results (holes) in the generalized Bloch sphere, which renders any trivial generalization ineffective [62]. The radius of this generalized Bloch sphere is given by $r = \sqrt{\frac{N}{N-1}\left(R - \frac{1}{N}\right)}$ [63], where $R = \mathrm{tr}(\rho^2)$.

The usual probability distribution computed from Eq. (3) for a walker performing CTQW on a ring of $N = 100$ nodes after some time $t = 10$ is shown in Fig. 5, which is similar to a CTQW walk distribution on a line for a short time and large N.[5] For simplicity, we have considered $\mu = 1$ [13], which
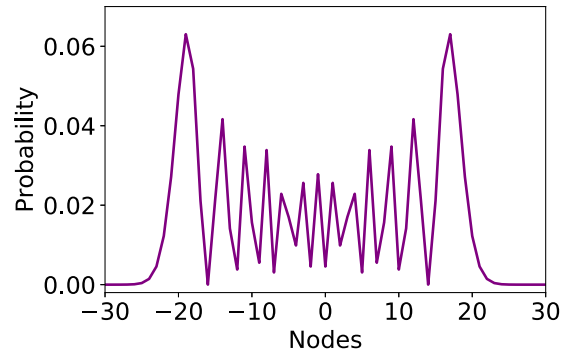

FIG. 5. Probability distribution for a single quantum walker on a ring of 100 nodes. The walker was initiated at node 50, and the probability distribution is after $t = 10$. In this diagram, node 50 is shifted to node 0.

means an unbiased transition to any adjacent vertex in an undirected graph $\mathcal{G}$ with no loops.[6] The density matrix of the walker at any time can be described using the standard basis as

$$\rho^t = \sum_i p_i^t |i\rangle\langle i|, \quad (25)$$

where p_i^t is the probability of finding the walker on a node (vertex) i after some time t since the walk was initiated. As we have already described, the Laplacian of $\mathcal{G}$ can be expressed as

$$\begin{aligned}\mathbf{L} &= \mathbf{D} - \mathbf{A} \\ &= \sum_{ij}[d_i\delta_{ij}|i\rangle\langle j| - \mathbb{E}_{ij}(|i\rangle\langle j| + |j\rangle\langle i|)],\end{aligned} \quad (26)$$

where $\mathbb{E}_{ij} = 1$ when there is an edge element $e_{ij} \in \mathbb{E}$, and zero otherwise. We notice from the Hamiltonian presented in the standard basis that the diagonal elements are simply the degree matrix entries, $H_{ii}^d = \mu d_i$, and d_i is the degree at the vertex v_i. So in the case of these walks, using the computation of β_i carried out in Appendix D, Eq. (16) becomes

$$\rho^t = \exp(-i\mathcal{H}t)\left(\sum_m \exp(\eta_m^t - \eta_m^c)\mathbb{P}_m\right)\exp(i\mathcal{H}t), \quad (27)$$

where $\eta_m^t = [\ln(p_m^0) + \eta_m^c]e^{-t/\tau} = \tilde{v}_i\eta_t$, and $\eta_m^c = \mu\beta_H d_i - \beta_I$, and $\mathbb{P}_m$ is the projection operator as before. p_m^0 is found using Eq. (18). We use the predefined parameters to model the walk to understand what is happening and whether the solution (27) is meaningful. A cycle graph $\mathcal{C}_N$ being 2-regular has the following Hamiltonian in the standard basis:

$$\mathcal{H} = \sum_i[2|i\rangle\langle i| - \mathbb{E}_{i,\tilde{i}}(|i\rangle\langle\tilde{i}| + |\tilde{i}\rangle\langle i|)], \quad (28)$$

---

[5]It is to be noted while we find probability distributions such as this at some time t, they are not the same for the discrete and con-

tinuous case. In the continuous case, we have transition amplitudes per unit time (μ), and we consider probabilities at some instance post-initiation. These instances can be recorded as *steps*. Wherein for the discrete case, a coin operation followed by a swap operation constitutes a *step*.

[6]In Fig. 5 we have shown only the nodes up to which the walker has spread after $t = 10$; it does not show all nodes.
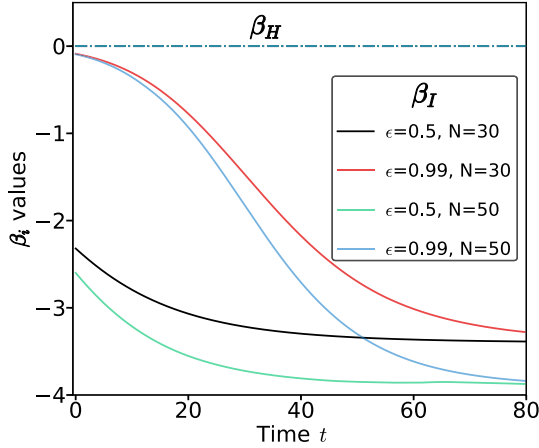
FIG. 6. Plot of β_i vs time. In the legend, β_I is tagged, as it varies for different N and ε values. β_H is the constant line $y = 0$.

where $\tilde{i} = i \pmod{N} + 1$. Using this $\mathcal{H}$, and the equilibrium distribution ρ_u, we get from Eq. (D1) the limiting β_i values which we use for CTQW (here we are interested in the equilibrium behavior),

$$\beta_H = 0,$$
$$\beta_I = -\ln(N), \tag{29}$$

where $k = 1$. In Fig. 6 we plot the variation of β_I for two different N values of 50 and 30, respectively. We numerically solve Eq. (8) and use the ρ thus produced at each iteration to compute β_i's as defined in Appendix B. This plot suggests that β_I assumes a final value dependent on N and the mean energy. Consider the red and black lines, for instance. As time progresses, we see that they merge towards a fixed value which is given by Eq. (29), suggesting that even though there is an initial dependence on ε, as equilibrium approaches, all of the β_I's assume the same value. Considering the initial β_i in FLM will be prudent if one wishes to study the behavior far from equilibrium. Otherwise, fixing the multipliers at an equilibrium distribution to use for FLM will faithfully represent equilibrium behavior. The β_H plot is shown by the $y = 0$ line in the graph, which remains constant in this case. The variation in β_I lies within a single order of magnitude and does not reflect a strong difference in probability amplitudes, as seen in Fig. 7.

Using appropriate τ values, we get the probability distributions as plotted in Fig. 7. Here it is not easy to discern between results from the FLM (solid lines) and those from the numerical solution of Eq. (8). The typical values of probability amplitudes lie within the order of 10^{-2} as seen in the plot. From our numerical computation, we have estimated the difference with FLM results, which is of the order 10^{-4} for low τ and of the order 10^{-3} for high τ's. We see that, for the distributions considered after $t = 20$, a similarity in the behavior of probability emerges as in Figs. 2 and 3(a). Higher τ or states closer to unitary states tend to relax slower. For low enough τ, the rapid relaxation of the system is observed in Fig. 7, and all initial information is lost. On the other hand, high τ states having lesser entropy generation rates drive the system toward unitary-like behavior. This can also be
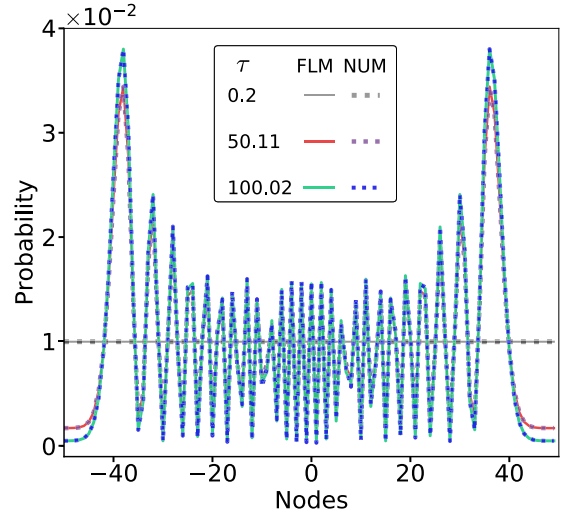

FIG. 7. Probability distribution for a single quantum walker on a ring of 100 nodes under SEA conditions, initiated at node 50 (shifted to node 0 for symmetry), after $t = 20$. The relaxation time τ is 0.2, 50.11, and 100.02 (first column in the legend), respectively. ε is 0.99. The plot contains both results from plotting the analytic solution found using the FLM method (solid lines in the plot) and those (dotted lines in the plot above) from the numerical solution to Eq. (8) using a CTQW Hamiltonian and other relevant substitutions.

understood in terms of localization and delocalization of the walker. The probability distribution for the case of $\tau = 0.2$ in Fig. 7 shows strong delocalisation. Whereas in the same figure, because of $\tau = 50.11$, 100.02, and $t = 20 < \tau$, we can say decoherence is yet to set in; that is, it displays linear behavior. As understood so far, low τ results in more nonlinear behavior. But how low? Unfortunately, the answer to such a question remains elusive [45]. Yet we can try to identify such low τ domains of high entropy generation by plotting the rate of entropy generation Π_S (A7) against τ and ε values as given in Fig. 8 for a CTQW with $N = 50$. The leading contribution in determining Π_S comes from τ; one can confirm from Fig. 8 that higher relaxation time represents almost zero entropy generation agreeing with our previous results. Lower τ states produce higher Π_S values early, as seen in Fig. 8(a), which is a typical SEA behavior. Also, as time progresses, these highest Π_S states (bounded by the cyan line in the plots) start moving up along the right side of the diagram as in Fig. 8(b). At a later time, only large τ-valued states are yet to equilibrate, resulting in a change in entropy. Note that the quantity ε by construction represents how pure the initial state is. So it is expected for a state with low ε to reach equilibrium (that is, a noisy state becomes noisier) rather fast. Yet the entropy production may not be maximum in those cases, as seen in Fig. 8. States relatively close to the pure states show a maximum entropy production rate under SEA evolution (the deep purple-shaded contours in the diagram). This behavior should be attributed to the fact that in the Bloch sphere representation, the low entropic states lying far away from equilibrium have to go through a greater change in entropy while equilibrating. Thus, their low information content accounts for a low entropy generation rate despite noisy channels becoming noisier.
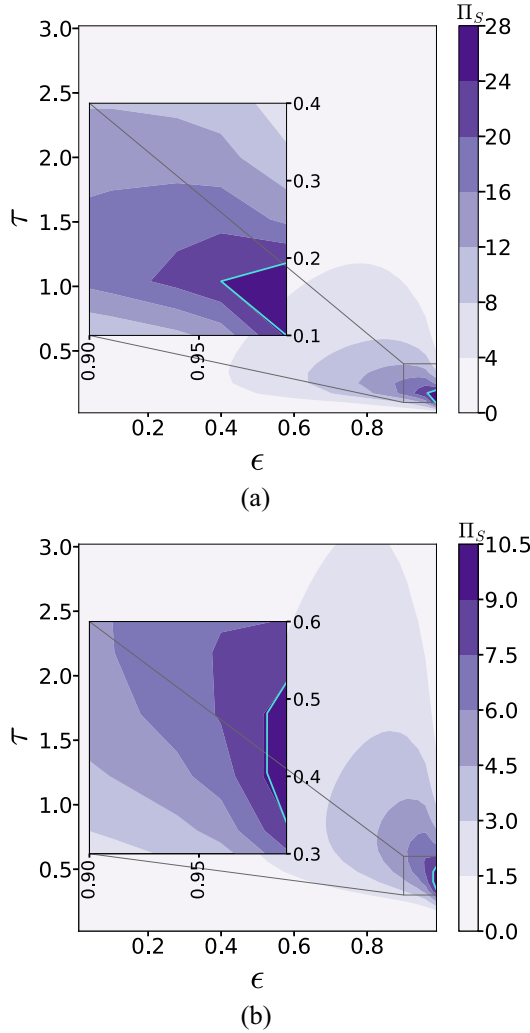
FIG. 8. Π_S distribution for a CTQW of $N = 50$ over different τ and ε values after time $t = 1$ (a) and $t = 3$ (b). The color bars provide the range and contrast of Π_S values. As discussed in the main text, the high Π_S-valued zones are concentrated around high ε and low τ values. These deep purple areas bounded in cyan represent the maximum entropy generation area. Insets of panels (a) and (b): zoomed-in view of the bounded region displaying max Π_S.

We also run some consistency checks to validate our FLM results against numerical solutions of Eq. (9), such as computing average energy [Fig. 9(a)], plotting entropy vs time [Fig. 9(b)], and entropy generation rate vs time as shown in Fig. 10. As before, we see a good agreement between the numerical and FLM results in Figs. 9 and 10. As the average energy remains constant throughout the walk [Fig. 9(a)], we see entropy increasing monotonically and saturating at the maximum value [Fig. 9(b)]. As we observe later, slight disagreements between full numerical (NUM in the plot) and FLM start appearing (blue dotted and green solid line in the plot). In this panel, we also see that almost instantaneously, the lowest τ valued line (black and gray ones in the plot) reaches maximum entropy. To see the corresponding rate of change of S, we turn to Fig. 10(a), where we see within $t < 0.1$ the graph peaks around the value 32, which is twice the order of magnitude higher in other high-τ cases [Fig. 10(b)]. This
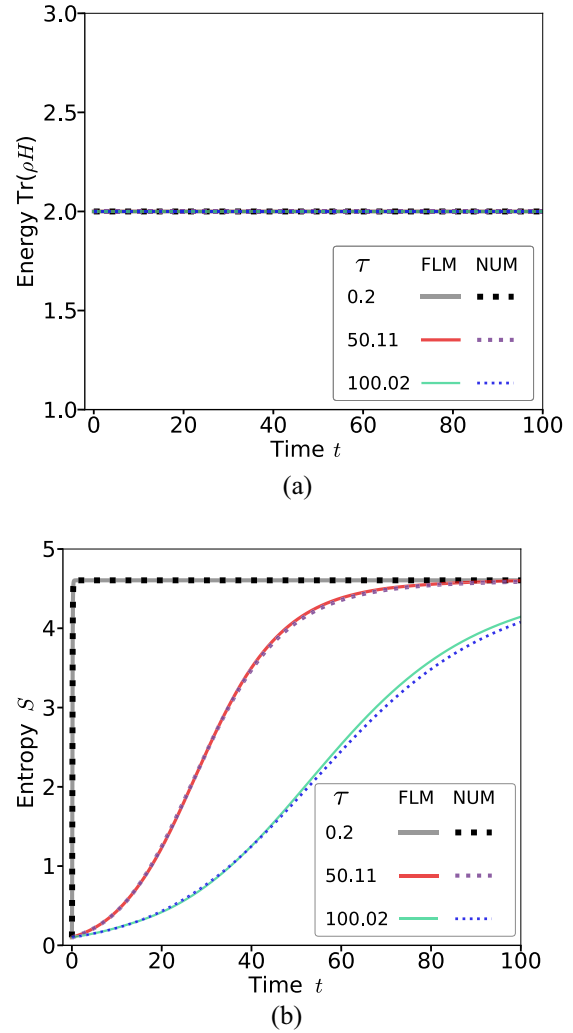

FIG. 9. (a) Plot of average energy vs time and (b) entropy vs time for a CTQW on a cycle graph of 100 nodes for various τ (first column of the legend) values and $\varepsilon = 0.99$. The walk was performed up to $t = 100$. FLM (solid lines) denotes the analytically computed results, while NUM (dotted lines) denotes numerical results.

supports the SEA ansatz that the steepest entropic path is also the one with maximum entropy production rate, and this happens at low τ values. Also, as noticed in Fig. 2, as τ increases, we see differences between FLM and NUM results.

IV. DISCUSSION AND CONCLUSION

Let us recapitulate what we have presented here. Our goal was to find spontaneously dissipative solutions to a continuous-time quantum walker (CTQW). In search of a suitable theory to characterize such dissipation, we arrive at the nonequilibrium thermodynamics propagated by Beretta and his co-workers under the name the steepest entropy ascent (SEA) ansatz or local-SEA (LSEA) [49]. This theory entails a local description of the system and arrives at nonlinear dynamics without invoking a heat bath or phenomenological tools such as presented by GENERIC dynamics. While these two approaches remain seemingly different in concept and application, in reality, it is not the case [53]. Hence, we
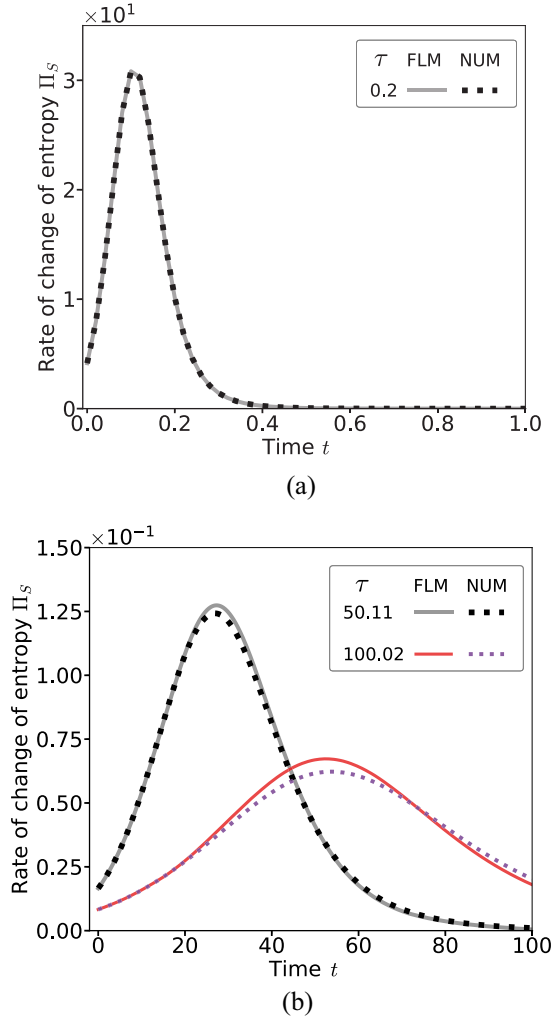
FIG. 10. Plot of rate of change of entropy vs time for a CTQW on a cycle graph of 100 nodes for (a) $\tau = 0.2$ and (b) $\tau = (50.11, 100.02)$ with $\varepsilon = 0.99$. FLM (solid lines) denotes the analytically computed results, while NUM (dotted lines) denotes numerical results.

choose SEA dynamics to govern dissipation in our CTQW system. The SEA principle can also be termed the fourth law of thermodynamics [50], which guarantees a unique global stable state with maximum entropy and all other states to be nonstable, metastable, or limit cycles. The SEA ansatz describes motion towards such a stable state under the local maximum entropy production principle by respecting the conservation laws. In that spirit, this work is a study of a single-particle quantum system as a consequence of the fourth law of thermodynamics.

The nonlinearity introduced in the general EoM of the SEA evolution renders any analytical attempt at a general solution highly difficult. Various special cases have been considered in literature till now. Herein, we provide a different approach by considering fixed Lagrange's multipliers (FLM) throughout the evolution under SEA within a good approximation of the numerical results. We have arrived at a solution that can be applied to varied cases. Our first example is a qubit. Despite being a simple system, it has been sparsely discussed in the SEA literature; we expound on that here. We have rederived the solutions from our general equation (8) using FLM on a Bloch sphere. From the magnitude of the Bloch vector vs time plot, we see the effect of SEA dynamics in Fig. 2. We observe a strong dependence of dissipation on the system's intrinsic relaxation time τ. High τ means if $t \ll \tau$, the system is yet to relax and unitary dynamics dominate the evolution, resulting in the quantum limit of the SEA dynamics. At the other extreme, for small but positive τ, there is a rapid ascent towards the maximally mixed state, which is evident in the equatorial plot of Fig. 3(a). As the entropy generation rate is inversely related to τ, this is also the domain of maximum entropy production. Here the system relaxes effectively instantaneously. Our approximate analytical result using FLM is an approximate result that agrees with the existing result due to Beretta [43] (GPB lines). The difference between GPB and FLM results in Fig. 2 originates from fixing multipliers. Although it is an approximate result, FLM works satisfactorily for two-level systems and d-level ones. FLM shows the agreement in Fig. 2, giving us confidence in our approach.

We consider a similar analysis for SEA on a single CTQW, which is an N-level extension of the qubit case. In Fig. 7 we compare our FLM results with the full numerical solution and find good agreement. We also plot the rate of entropy generation against ε and τ and map the plot with contours. Low τ and high ε cases showed a high rate of entropy generating contours, as seen in Fig. 8. We identify such regions of τ-ε where SEA dynamics dominate [see insets of Figs. 8(a) and 8(b)]. These are the states residing near the $\text{tr}(\rho^2) = 1$ showing maximum entropy generation in this figure. However, these marked domains in Fig. 8 change with time, as different τ values activate Π_S at different times, as seen in Fig. 10. So the goal of estimating a lower bound on τ has turned into a time-dependent problem; that is, for initial times, look at low τ for max entropy generation, and at later times look towards higher τ values. The agreement between FLM and numerical results continues to hold even when we compare average energy, entropy, and entropy growth over time in Figs. 9 and 10. This shows the robustness of the FLM approach against various conditions.

Kendon and Tregenna [25] found decoherence to be helpful in quantum walks in their famous work. They introduced decoherence via weak measurements on each vertex. Instead, here, we do that via the SEA framework. We find that decoherence is useful in quantum walks. However, it can also be useful when the relaxation time of the system is short as it facilitates mixing. This paper shows that SEA with FLM can be used in many scenarios. This work raises further questions regarding the effect on QW's mixing time under such SEA dynamics. One may venture into the multiwalker case from here and seek to study various separability criteria that may be exploited.
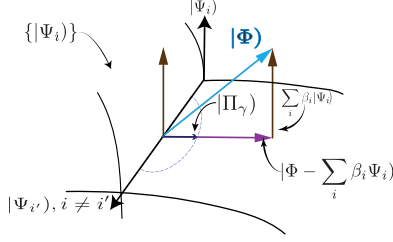
FIG. 11. Geometric interpretation of the SEA principle. The manifold $\mathscr{L}$ is spanned by the set $\{|\Psi_i\rangle\}$, which is shown as encoded on a surface, whose spanning vectors are shown along the edges. $|\Phi\rangle$ is the entropy gradient functional whose projection on the plane perpendicular to $\mathscr{L}$ provides the direction of motion under SEA (purple arrow), while the magnitude of Π_γ is constrained by a suitable value set to Eq. (A2), $\frac{dl}{dt} = \dot{\epsilon}$, which defines a circle in the orthogonal plane, shown dotted in the diagram [52].

APPENDIX A: DERIVATION OF SEA EOM

In this Appendix we sketch the basic derivation of the SEA equation of motion (EOM); by no means this is a complete formulation of what SEA pertains to (see the references in the main text for that purpose), but rather a guide to what is usually done.

The state operator γ's rate of change follows the given equation [57]:

$$\dot{\gamma} = \dot{\gamma}_H + \dot{\gamma}_D, \tag{A1}$$

where $\dot{\gamma}_H$ represents evolution under purely Hamiltonian considerations and $\dot{\gamma}_D$ represents the same due to dissipation. While $\dot{\gamma}_H$ can be written using Schrödinger's equation, the other component requires SEA formalism. Having defined the gradients in the main text [see Eqs. (5) and (6)], we can associate the following geometrical notion to this motion. Let us consider Fig. 11: the conservation quantities and constraints of the motion span the linear manifold $\{|\Psi_i\rangle\}$, and the entropy functional and γ resides in the plane orthogonal to it [52]. The gradient of the entropy functional, the steepest ascent aspect, projects the two components, as shown in the figure. Our interest is in the component perpendicular to the manifold spanned by $|\Psi_i\rangle$s, denoted by the purple arrow in the diagram.

To fix the norm of the rate of change of γ, one includes the metric in the following fashion [52]:

$$dl = \sqrt{(\Pi_\gamma \mid \hat{G}(\gamma) \mid \Pi_\gamma)} dt. \tag{A2}$$

Thus, we have one more constraint.

Returning to the derivation, we can write the constraints using Lagrange multipliers in the following form:

$$\Upsilon = \Pi_S - \sum_i \bar{\beta}_i \Pi_{C_i} - \frac{\tau}{2}(\Pi_\gamma \mid \hat{G}(\gamma) \mid \Pi_\gamma), \tag{A3}$$

where $\bar{\beta}_i$ and $\tau/2$ are Lagrange multipliers independent of Π_γ. The above equation can be reshaped using Eqs. (5) and (6), and then on taking the functional derivative of Υ with respect to $|\Pi_\gamma)$ we get

$$\frac{\delta \Upsilon}{\delta \Pi_\gamma} = |\Phi\rangle - \sum_i \bar{\beta}_i |\Psi_i\rangle - \tau \hat{G}(\gamma)|\Pi_\gamma). \tag{A4}$$

The equation of motion for γ, $\dot{\gamma}_D$ to be precise, i.e., Eq. (7) is found setting $\frac{\delta \Upsilon}{\delta \Pi_\gamma} = 0$ as shown below:

$$|\Pi_\gamma) = \mathcal{L}\left|\Phi - \sum_i \bar{\beta}_i \Psi_i\right). \tag{A5}$$

$\mathcal{L}$ is given by $\frac{1}{\tau}\hat{G}(\gamma)^{-1}$, and it behaves as a superoperator with the properties $\mathcal{L}(A)B = \mathcal{L}(AB)$ and $[\mathcal{L}(A)]^\dagger = A^\dagger \mathcal{L}$. For the purpose of our problem, we use $\mathcal{L} = \frac{1}{4k\tau}\mathrm{I}$ (I the Fisher metric, k to counter the k in entropy, and 4 for scaling). To derive Eq. (8), we begin by using the following relation for dissipative motion:

$$\frac{d\rho_D}{dt} = \Pi_\gamma \gamma^\dagger + \gamma \Pi_{\gamma^\dagger} = \dot{\gamma}_D \gamma^\dagger + \gamma \dot{\gamma}_D^\dagger.$$

We get using Eq. (7) along with the equation above, together with the definitions- $|\Phi\rangle = |\delta \mathbf{S}(\gamma)/\delta \gamma\rangle = |-2k(\ln \gamma \gamma^\dagger + 1)\gamma\rangle$ and $|\Psi_i\rangle = |\delta \mathbf{C_i}(\gamma)/\delta \gamma\rangle = |2\mathbf{C_i}\gamma\rangle$, to get the following expression for the dissipative part of the dynamics:

$$\Pi_\gamma = -2\mathcal{L}\left|k \ln(\gamma \gamma^\dagger + 1)\gamma + \sum_i \bar{\beta}_i \mathbf{C_i}\gamma\right),$$

$$\text{using } \frac{d\rho_D}{dt} = \Pi_\gamma \gamma^\dagger + \gamma \Pi_{\gamma^\dagger},$$

$$\frac{d\rho_D}{dt} = -2\bigg[k\mathcal{L}[\ln(\gamma \gamma^\dagger)]\gamma \gamma^\dagger + \sum_i \bar{\beta}_i \mathcal{L}(\mathbf{C_i})\gamma \gamma^\dagger + k\mathcal{L}\gamma \gamma^\dagger$$

$$+ k\gamma \gamma^\dagger \mathcal{L} + k\gamma \gamma^\dagger \ln(\gamma \gamma^\dagger)\mathcal{L} + \sum_i \bar{\beta}_i \gamma \gamma^\dagger \mathbf{C_i}\mathcal{L}\bigg].$$

Identifying $\gamma \gamma^\dagger = \rho$, we can rearrange the r.h.s. of the last statement of the above equation to get the following one:

$$\frac{d\rho_D}{dt} = -2\bigg[k\{\mathcal{L}[\ln(\rho)], \rho\} + k\{\mathcal{L}, \rho\} + \sum_i \bar{\beta}_i \{\mathcal{L}(\mathbf{C_i}), \rho\}\bigg]. \tag{A6}$$

Similarly, using Schrödinger's equation, we find

$$\dot{\gamma}_H = -\frac{i}{\hbar}\mathcal{H}\gamma.$$

Now, using $\dot{\rho} = \dot{\gamma}\gamma^\dagger + \gamma\dot{\gamma}^\dagger$, $\hbar = 1$, and Eq. (A1) and (A6), we get Eqs. (4) and (8).

A useful term in our analysis is Π_S, the entropy generation rate functional from Eq. (5). It is given by

$$
\begin{aligned}
\Pi_S &= -k\frac{d\mathrm{tr}[\rho\ln(\rho)]}{dt} \\
&= -k\mathrm{tr}\left[(\ln(\rho)+1)\frac{d\rho}{dt}\right] \\
&= 2k^2\mathrm{tr}[(\ln(\rho)+1]\mathcal{L}\{\ln(\rho),\rho\}) \\
&\quad + 2k^2\sum_i(-1)^i\beta_i\mathrm{tr}\{[\ln(\rho)+1]\mathcal{L}\{\mathbf{C_i},\rho\}\}.
\end{aligned} \tag{A7'}
$$

The β_i is scaled in the above equation [see Eqs. (B11)–(B13) below]. Using $\mathcal{L} = \frac{1}{4k\tau}$, we get

$$
\begin{aligned}
\Pi_S &= \frac{k}{2\tau}(\mathrm{tr}\{[\ln(\rho)+1]\{\ln(\rho),\rho\}\} \\
&\quad + \sum_i(-1)^i\beta_i\mathrm{tr}\{[\ln(\rho)+1]\{\mathbf{C_i},\rho\}\}).
\end{aligned} \tag{A7}
$$

APPENDIX B: DETERMINING LAGRANGE MULTIPLIERS

Using the constraints of Eqs. (5)–(7) we get

$$
\sum_i(\Psi_j|\mathcal{L}|\Psi_i)\bar{\beta}_i = k(\Psi_j|\mathcal{L}|\Phi). \tag{B1}
$$

This equation can be solved using Cramer's rule for solving linear equation with multiple variables, provided the solution exists ($\bar{\Omega} = \det(\Delta) \neq 0$), which is equivalent to the following expression (considering three constraints and corresponding three $\bar{\beta}$s):

$$
\bar{\Omega} = \begin{vmatrix} (\Psi_1 \mid \mathcal{L} \mid \Psi_1) & (\Psi_1 \mid \mathcal{L} \mid \Psi_2) & (\Psi_1 \mid \mathcal{L} \mid \Psi_3) \\ (\Psi_2 \mid \mathcal{L} \mid \Psi_1) & (\Psi_2 \mid \mathcal{L} \mid \Psi_2) & (\Psi_2 \mid \mathcal{L} \mid \Psi_3) \\ (\Psi_3 \mid \mathcal{L} \mid \Psi_1) & (\Psi_3 \mid \mathcal{L} \mid \Psi_2) & (\Psi_3 \mid \mathcal{L} \mid \Psi_3) \end{vmatrix},
$$

$$
\bar{\beta}_1 = \frac{1}{\bar{\Omega}} \begin{vmatrix} (\Psi_1 \mid \mathcal{L} \mid \Phi) & (\Psi_1 \mid \mathcal{L} \mid \Psi_2) & (\Psi_1 \mid \mathcal{L} \mid \Psi_3) \\ (\Psi_2 \mid \mathcal{L} \mid \Phi) & (\Psi_2 \mid \mathcal{L} \mid \Psi_2) & (\Psi_2 \mid \mathcal{L} \mid \Psi_3) \\ (\Psi_3 \mid \mathcal{L} \mid \Phi) & (\Psi_3 \mid \mathcal{L} \mid \Psi_2) & (\Psi_3 \mid \mathcal{L} \mid \Psi_3) \end{vmatrix},
$$

$$
\bar{\beta}_2 = \frac{1}{\bar{\Omega}} \begin{vmatrix} (\Psi_1 \mid \mathcal{L} \mid \Psi_1) & (\Psi_1 \mid \mathcal{L} \mid \Phi) & (\Psi_1 \mid \mathcal{L} \mid \Psi_3) \\ (\Psi_2 \mid \mathcal{L} \mid \Psi_1) & (\Psi_2 \mid \mathcal{L} \mid \Phi) & (\Psi_2 \mid \mathcal{L} \mid \Psi_3) \\ (\Psi_3 \mid \mathcal{L} \mid \Psi_1) & (\Psi_3 \mid \mathcal{L} \mid \Phi) & (\Psi_3 \mid \mathcal{L} \mid \Psi_3) \end{vmatrix},
$$

$$
\bar{\beta}_3 = \frac{1}{\bar{\Omega}} \begin{vmatrix} (\Psi_1 \mid \mathcal{L} \mid \Psi_1) & (\Psi_1 \mid \mathcal{L} \mid \Psi_2) & (\Psi_1 \mid \mathcal{L} \mid \Phi) \\ (\Psi_2 \mid \mathcal{L} \mid \Psi_1) & (\Psi_2 \mid \mathcal{L} \mid \Psi_2) & (\Psi_2 \mid \mathcal{L} \mid \Phi) \\ (\Psi_3 \mid \mathcal{L} \mid \Psi_1) & (\Psi_3 \mid \mathcal{L} \mid \Psi_2) & (\Psi_3 \mid \mathcal{L} \mid \Phi) \end{vmatrix}. \tag{B2}
$$

On column rearrangement, we get

$$
\bar{\beta}_2 = -\frac{1}{\bar{\Omega}} \begin{vmatrix} (\Psi_1 \mid \mathcal{L} \mid \Phi) & (\Psi_1 \mid \mathcal{L} \mid \Psi_1) & (\Psi_1 \mid \mathcal{L} \mid \Psi_3) \\ (\Psi_2 \mid \mathcal{L} \mid \Phi) & (\Psi_2 \mid \mathcal{L} \mid \Psi_1) & (\Psi_2 \mid \mathcal{L} \mid \Psi_3) \\ (\Psi_3 \mid \mathcal{L} \mid \Phi) & (\Psi_3 \mid \mathcal{L} \mid \Psi_1) & (\Psi_3 \mid \mathcal{L} \mid \Psi_3) \end{vmatrix},
$$

$$
\bar{\beta}_3 = \frac{1}{\bar{\Omega}} \begin{vmatrix} (\Psi_1 \mid \mathcal{L} \mid \Phi) & (\Psi_1 \mid \mathcal{L} \mid \Psi_1) & (\Psi_1 \mid \mathcal{L} \mid \Psi_2) \\ (\Psi_2 \mid \mathcal{L} \mid \Phi) & (\Psi_2 \mid \mathcal{L} \mid \Psi_1) & (\Psi_2 \mid \mathcal{L} \mid \Psi_2) \\ (\Psi_3 \mid \mathcal{L} \mid \Phi) & (\Psi_3 \mid \mathcal{L} \mid \Psi_1) & (\Psi_3 \mid \mathcal{L} \mid \Psi_2) \end{vmatrix}.
$$

Before explicitly finding out the $\bar{\beta}_i$s, let us consider Eq. (A5), and substitute $\bar{\beta}_i$'s to get the following equation [52]:

$$
\begin{aligned}
\Pi_\gamma &= \mathcal{L}(\Phi)\frac{\bar{\Omega}}{\bar{\Omega}} - \frac{\mathcal{L}}{\bar{\Omega}} \begin{vmatrix} (\Psi_1 \mid \mathcal{L} \mid \Phi) & (\Psi_1 \mid \mathcal{L} \mid \Psi_2) & (\Psi_1 \mid \mathcal{L} \mid \Psi_3) \\ (\Psi_2 \mid \mathcal{L} \mid \Phi) & (\Psi_2 \mid \mathcal{L} \mid \Psi_2) & (\Psi_2 \mid \mathcal{L} \mid \Psi_3) \\ (\Psi_3 \mid \mathcal{L} \mid \Phi) & (\Psi_3 \mid \mathcal{L} \mid \Psi_2) & (\Psi_3 \mid \mathcal{L} \mid \Psi_3) \end{vmatrix}(\Psi_1) \\
&\quad + \frac{\mathcal{L}}{\bar{\Omega}} \begin{vmatrix} (\Psi_1 \mid \mathcal{L} \mid \Phi) & (\Psi_1 \mid \mathcal{L} \mid \Psi_1) & (\Psi_1 \mid \mathcal{L} \mid \Psi_3) \\ (\Psi_2 \mid \mathcal{L} \mid \Phi) & (\Psi_2 \mid \mathcal{L} \mid \Psi_1) & (\Psi_2 \mid \mathcal{L} \mid \Psi_3) \\ (\Psi_3 \mid \mathcal{L} \mid \Phi) & (\Psi_3 \mid \mathcal{L} \mid \Psi_1) & (\Psi_3 \mid \mathcal{L} \mid \Psi_3) \end{vmatrix}(\Psi_2) - \frac{\mathcal{L}}{\bar{\Omega}} \begin{vmatrix} (\Psi_1 \mid \mathcal{L} \mid \Phi) & (\Psi_1 \mid \mathcal{L} \mid \Psi_1) & (\Psi_1 \mid \mathcal{L} \mid \Psi_2) \\ (\Psi_2 \mid \mathcal{L} \mid \Phi) & (\Psi_2 \mid \mathcal{L} \mid \Psi_1) & (\Psi_2 \mid \mathcal{L} \mid \Psi_2) \\ (\Psi_3 \mid \mathcal{L} \mid \Phi) & (\Psi_3 \mid \mathcal{L} \mid \Psi_1) & (\Psi_3 \mid \mathcal{L} \mid \Psi_2) \end{vmatrix}(\Psi_3),
\end{aligned} \tag{B3}
$$

$$
\Pi_\gamma = \frac{\begin{vmatrix} \mathcal{L}(\Phi) & \mathcal{L}(\Psi_1) & \mathcal{L}(\Psi_2) & \mathcal{L}(\Psi_3) \\ (\Psi_1 \mid \mathcal{L} \mid \Phi) & (\Psi_1 \mid \mathcal{L} \mid \Psi_1) & (\Psi_1 \mid \mathcal{L} \mid \Psi_2) & (\Psi_1 \mid \mathcal{L} \mid \Psi_3) \\ (\Psi_2 \mid \mathcal{L} \mid \Phi) & (\Psi_2 \mid \mathcal{L} \mid \Psi_1) & (\Psi_2 \mid \mathcal{L} \mid \Psi_2) & (\Psi_2 \mid \mathcal{L} \mid \Psi_3) \\ (\Psi_3 \mid \mathcal{L} \mid \Phi) & (\Psi_3 \mid \mathcal{L} \mid \Psi_1) & (\Psi_3 \mid \mathcal{L} \mid \Psi_2) & (\Psi_3 \mid \mathcal{L} \mid \Psi_3) \end{vmatrix}}{\begin{vmatrix} (\Psi_1 \mid \mathcal{L} \mid \Psi_1) & (\Psi_1 \mid \mathcal{L} \mid \Psi_2) & (\Psi_1 \mid \mathcal{L} \mid \Psi_3) \\ (\Psi_2 \mid \mathcal{L} \mid \Psi_1) & (\Psi_2 \mid \mathcal{L} \mid \Psi_2) & (\Psi_2 \mid \mathcal{L} \mid \Psi_3) \\ (\Psi_3 \mid \mathcal{L} \mid \Psi_1) & (\Psi_3 \mid \mathcal{L} \mid \Psi_2) & (\Psi_3 \mid \mathcal{L} \mid \Psi_3) \end{vmatrix}}. \tag{B4}
$$

To find a more comprehensive expression, we make use of the following relations:

$$
\begin{aligned}
(\Psi_i \mid \mathcal{L} \mid \phi) &= -\frac{1}{\tau}\left(\mathrm{tr}\left[\rho\frac{1}{2}\{\mathbf{C_i},\ln(\rho)\}\right] + \mathrm{tr}\left(\frac{1}{2}\{\mathbf{C_i},\rho\}\right)\right), \\
(\Psi_i \mid \mathcal{L} \mid \Psi_j) &= \frac{1}{k\tau}\mathrm{tr}\left(\rho\frac{1}{2}\{\mathbf{C_i},\mathbf{C_j}\}\right).
\end{aligned} \tag{B5}
$$

Using these relations, we find the expressions for $\bar{\beta}_i$ from Eq. (B2) as follows:

$$
\bar{\Omega} = \frac{1}{(k\tau)^3} \begin{vmatrix} \mathrm{tr}(\frac{\rho}{2}\{\mathbf{C_1},\mathbf{C_1}\}) & \mathrm{tr}(\frac{\rho}{2}\{\mathbf{C_1},\mathbf{C_2}\}) & \mathrm{tr}(\frac{\rho}{2}\{\mathbf{C_1},\mathbf{C_3}\}) \\ \mathrm{tr}(\frac{\rho}{2}\{\mathbf{C_2},\mathbf{C_1}\}) & \mathrm{tr}(\frac{\rho}{2}\{\mathbf{C_2},\mathbf{C_2}\}) & \mathrm{tr}(\frac{\rho}{2}\{\mathbf{C_2},\mathbf{C_3}\}) \\ \mathrm{tr}(\frac{\rho}{2}\{\mathbf{C_3},\mathbf{C_1}\}) & \mathrm{tr}(\frac{\rho}{2}\{\mathbf{C_3},\mathbf{C_2}\}) & \mathrm{tr}(\frac{\rho}{2}\{\mathbf{C_3},\mathbf{C_3}\}) \end{vmatrix}, \tag{B6}
$$

$$\bar{\beta}_1 = -\frac{1}{k^2\tau^3\bar{\Omega}}\begin{vmatrix} \mathrm{tr}[\frac{\rho}{2}\{\mathbf{C_1},\ln(\rho)+1\}] & \mathrm{tr}(\frac{\rho}{2}\{\mathbf{C_1},\mathbf{C_2}\}) & \mathrm{tr}(\frac{\rho}{2}\{\mathbf{C_1},\mathbf{C_3}\}) \\ \mathrm{tr}[\frac{\rho}{2}\{\mathbf{C_2},\ln(\rho)+1\}] & \mathrm{tr}(\frac{\rho}{2}\{\mathbf{C_2},\mathbf{C_2}\}) & \mathrm{tr}(\frac{\rho}{2}\{\mathbf{C_2},\mathbf{C_3}\}) \\ \mathrm{tr}[\frac{\rho}{2}\{\mathbf{C_3},\ln(\rho)+1\}] & \mathrm{tr}(\frac{\rho}{2}\{\mathbf{C_3},\mathbf{C_2}\}) & \mathrm{tr}(\frac{\rho}{2}\{\mathbf{C_3},\mathbf{C_3}\}) \end{vmatrix}, \tag{B7}$$

$$\bar{\beta}_2 = \frac{1}{k^2\tau^3\bar{\Omega}}\begin{vmatrix} \mathrm{tr}[\frac{\rho}{2}\{\mathbf{C_1},\ln(\rho)+1\}] & \mathrm{tr}(\frac{\rho}{2}\{\mathbf{C_1},\mathbf{C_1}\}) & \mathrm{tr}(\frac{\rho}{2}\{\mathbf{C_1},\mathbf{C_3}\}) \\ \mathrm{tr}[\frac{\rho}{2}\{\mathbf{C_2},\ln(\rho)+1\}] & \mathrm{tr}(\frac{\rho}{2}\{\mathbf{C_2},\mathbf{C_1}\}) & \mathrm{tr}(\frac{\rho}{2}\{\mathbf{C_2},\mathbf{C_3}\}) \\ \mathrm{tr}[\frac{\rho}{2}\{\mathbf{C_3},\ln(\rho)+1\}] & \mathrm{tr}(\frac{\rho}{2}\{\mathbf{C_3},\mathbf{C_1}\}) & \mathrm{tr}(\frac{\rho}{2}\{\mathbf{C_3},\mathbf{C_3}\}) \end{vmatrix}, \tag{B8}$$

$$\bar{\beta}_3 = -\frac{1}{k^2\tau^3\bar{\Omega}}\begin{vmatrix} \mathrm{tr}[\frac{\rho}{2}\{\mathbf{C_1},\ln(\rho)+1\}] & \mathrm{tr}(\frac{\rho}{2}\{\mathbf{C_1},\mathbf{C_1}\}) & \mathrm{tr}(\frac{\rho}{2}\{\mathbf{C_1},\mathbf{C_2}\}) \\ \mathrm{tr}[\frac{\rho}{2}\{\mathbf{C_2},\ln(\rho)+1\}] & \mathrm{tr}(\frac{\rho}{2}\{\mathbf{C_2},\mathbf{C_1}\}) & \mathrm{tr}(\frac{\rho}{2}\{\mathbf{C_2},\mathbf{C_2}\}) \\ \mathrm{tr}[\frac{\rho}{2}\{\mathbf{C_3},\ln(\rho)+1\}] & \mathrm{tr}(\frac{\rho}{2}\{\mathbf{C_3},\mathbf{C_1}\}) & \mathrm{tr}(\frac{\rho}{2}\{\mathbf{C_3},\mathbf{C_2}\}) \end{vmatrix}. \tag{B9}$$

We consider Eq. (A6) with $\mathcal{L} = \frac{1}{4k\tau}\mathrm{I}$, use the $\bar{\beta}_i$ from Eqs. (B6)–(B9), and after some algebra involving determinants, arrive at the equation below:

$$\frac{d\rho}{dt} + i[\mathcal{H},\rho] = -\frac{1}{\tau}\frac{\begin{vmatrix} \rho\ln(\rho) & \frac{1}{2}\{\mathbf{C_1},\rho\} & \frac{1}{2}\{\mathbf{C_2},\rho\} & \frac{1}{2}\{\mathbf{C_3},\rho\} \\ \mathrm{tr}[\frac{\rho}{2}\{\mathbf{C_1},\ln(\rho)\}] & \mathrm{tr}(\rho\mathbf{C_1}^2) & \mathrm{tr}(\frac{\rho}{2}\{\mathbf{C_1},\mathbf{C_2}\}) & \mathrm{tr}(\frac{\rho}{2}\{\mathbf{C_1},\mathbf{C_3}\}) \\ \mathrm{tr}[\frac{\rho}{2}\{\mathbf{C_2},\ln(\rho)\}] & \mathrm{tr}(\frac{\rho}{2}\{\mathbf{C_2},\mathbf{C_1}\}) & \mathrm{tr}(\rho\mathbf{C_2}^2) & \mathrm{tr}(\frac{\rho}{2}\{\mathbf{C_2},\mathbf{C_3}\}) \\ \mathrm{tr}[\frac{\rho}{2}\{\mathbf{C_3},\ln(\rho)\}] & \mathrm{tr}(\frac{\rho}{2}\{\mathbf{C_3},\mathbf{C_1}\}) & \mathrm{tr}(\frac{\rho}{2}\{\mathbf{C_3},\mathbf{C_2}\}) & \mathrm{tr}(\rho\mathbf{C_3}^2) \end{vmatrix}}{\begin{vmatrix} \mathrm{tr}(\frac{\rho}{2}\{\mathbf{C_1},\mathbf{C_1}\}) & \mathrm{tr}(\frac{\rho}{2}\{\mathbf{C_1},\mathbf{C_2}\}) & \mathrm{tr}(\frac{\rho}{2}\{\mathbf{C_1},\mathbf{C_3}\}) \\ \mathrm{tr}(\frac{\rho}{2}\{\mathbf{C_2},\mathbf{C_1}\}) & \mathrm{tr}(\frac{\rho}{2}\{\mathbf{C_2},\mathbf{C_2}\}) & \mathrm{tr}(\frac{\rho}{2}\{\mathbf{C_2},\mathbf{C_3}\}) \\ \mathrm{tr}(\frac{\rho}{2}\{\mathbf{C_3},\mathbf{C_1}\}) & \mathrm{tr}(\frac{\rho}{2}\{\mathbf{C_3},\mathbf{C_2}\}) & \mathrm{tr}(\frac{\rho}{2}\{\mathbf{C_3},\mathbf{C_3}\}) \end{vmatrix}}. \tag{B10}$$

Thus we have a full-fledged equation of motion in ρ under SEA. The β_i as given in Eqs. (B6)–(B9) can be rewritten in the following scaled form (using the scaling, $\bar{\Omega} = \frac{1}{(k\tau)^3}\Omega$):

$$\bar{\beta}_1 = -\frac{1}{k^2\tau^3\bar{\Omega}}\begin{vmatrix} \mathrm{tr}[\frac{\rho}{2}\{\mathbf{C_1},\ln(\rho)\}] & \mathrm{tr}(\frac{\rho}{2}\{\mathbf{C_1},\mathbf{C_2}\}) & \mathrm{tr}(\frac{\rho}{2}\{\mathbf{C_1},\mathbf{C_3}\}) \\ \mathrm{tr}[\frac{\rho}{2}\{\mathbf{C_2},\ln(\rho)\}] & \mathrm{tr}(\frac{\rho}{2}\{\mathbf{C_2},\mathbf{C_2}\}) & \mathrm{tr}(\frac{\rho}{2}\{\mathbf{C_2},\mathbf{C_3}\}) \\ \mathrm{tr}[\frac{\rho}{2}\{\mathbf{C_3},\ln(\rho)\}] & \mathrm{tr}(\frac{\rho}{2}\{\mathbf{C_3},\mathbf{C_2}\}) & \mathrm{tr}(\frac{\rho}{2}\{\mathbf{C_3},\mathbf{C_3}\}) \end{vmatrix} \tag{B11}$$

$$= -k\beta_1,$$

$$\bar{\beta}_2 = \frac{1}{k^2\tau^3\bar{\Omega}}\begin{vmatrix} \mathrm{tr}[\frac{\rho}{2}\{\mathbf{C_1},\ln(\rho)\}] & \mathrm{tr}(\frac{\rho}{2}\{\mathbf{C_1},\mathbf{C_1}\}) & \mathrm{tr}(\frac{\rho}{2}\{\mathbf{C_1},\mathbf{C_3}\}) \\ \mathrm{tr}[\frac{\rho}{2}\{\mathbf{C_2},\ln(\rho)\}] & \mathrm{tr}(\frac{\rho}{2}\{\mathbf{C_2},\mathbf{C_1}\}) & \mathrm{tr}(\frac{\rho}{2}\{\mathbf{C_2},\mathbf{C_3}\}) \\ \mathrm{tr}[\frac{\rho}{2}\{\mathbf{C_3},\ln(\rho)\}] & \mathrm{tr}(\frac{\rho}{2}\{\mathbf{C_3},\mathbf{C_1}\}) & \mathrm{tr}(\frac{\rho}{2}\{\mathbf{C_3},\mathbf{C_3}\}) \end{vmatrix}, \tag{B12}$$

$$= k\beta_2,$$

$$\bar{\beta}_3 = -\frac{1}{k^2\tau^3\bar{\Omega}}\begin{vmatrix} \mathrm{tr}[\frac{\rho}{2}\{\mathbf{C_1},\ln(\rho)\}] & \mathrm{tr}(\frac{\rho}{2}\{\mathbf{C_1},\mathbf{C_1}\}) & \mathrm{tr}(\frac{\rho}{2}\{\mathbf{C_1},\mathbf{C_2}\}) \\ \mathrm{tr}[\frac{\rho}{2}\{\mathbf{C_2},\ln(\rho)\}] & \mathrm{tr}(\frac{\rho}{2}\{\mathbf{C_2},\mathbf{C_1}\}) & \mathrm{tr}(\frac{\rho}{2}\{\mathbf{C_2},\mathbf{C_2}\}) \\ \mathrm{tr}[\frac{\rho}{2}\{\mathbf{C_3},\ln(\rho)\}] & \mathrm{tr}(\frac{\rho}{2}\{\mathbf{C_3},\mathbf{C_1}\}) & \mathrm{tr}(\frac{\rho}{2}\{\mathbf{C_3},\mathbf{C_2}\}) \end{vmatrix}, \tag{B13}$$

$$= -k\beta_3.$$

This allows us to write Eq. (A6) as follows:

$$\frac{d\rho_D}{dt} = -\frac{1}{\tau}\left[\rho\ln(\rho) + \frac{1}{2}\sum_i(-1)^i\beta_i\{\mathbf{C_i},\rho\}\right]. \tag{B14}$$

A single particle will require only two $\mathbf{C_i}$s; hence, modifying Eq. (B10) with appropriate constraints gets us the following equation:

$$\frac{d\rho}{dt} + i[\mathcal{H},\rho] = -\frac{1}{\tau}\frac{\begin{vmatrix} \rho\ln(\rho) & \rho & \frac{1}{2}\{\rho,\mathcal{H}\} \\ \mathrm{tr}[\rho\ln(\rho)] & 1 & \mathrm{tr}(\rho\mathcal{H}) \\ \mathrm{tr}[\rho\mathcal{H}\ln(\rho)] & \mathrm{tr}(\rho\mathcal{H}) & \mathrm{tr}(\rho\mathcal{H}^2) \end{vmatrix}}{\begin{vmatrix} 1 & \mathrm{tr}(\rho\mathcal{H}) \\ \mathrm{tr}(\rho\mathcal{H}) & \mathrm{tr}(\rho\mathcal{H}^2) \end{vmatrix}}. \tag{B15}$$

Considering qubits, as described in Sec. III B, we need to use the following traces as they appear in the equations for β_i in Eq. (B15). We use $\mathcal{H} = (\omega_0\mathrm{I} + \omega\hat{h}\cdot\vec{\sigma})$ and $\rho = \frac{1}{2}(\mathrm{I} + \vec{r}\cdot\vec{\sigma})$ as defined in the main text [43]. Defining $r_e = \hat{h}\cdot\vec{r}$ we get

$$\mathrm{tr}(\rho) = 1,$$

$$\mathrm{tr}(\rho\mathcal{H}) = (\omega_0 + \omega r_e),$$

$$\mathrm{tr}(\rho\mathcal{H}^2) = \left[(\omega^2 + \omega_0^2) + 2\omega_0\omega r_e\right],$$

$$\mathrm{tr}[\rho\ln(\rho)] = \frac{1}{2}\left[\ln\left(\frac{1-r^2}{4}\right) + r\ln\left(\frac{1+r}{1-r}\right)\right],$$

$$\mathrm{tr}[\rho\mathcal{H}\ln(\rho)] = \frac{\omega_0}{2}\left[\ln\left(\frac{1-r^2}{4}\right) + r\ln\left(\frac{1+r}{1-r}\right)\right]$$

$$+ \frac{\omega}{2} \left[\ln \left(\frac{1-r^2}{4} \right) + \frac{1}{r} \ln \left(\frac{1+r}{1-r} \right) \right] r_e.$$

One can plug these traces into the β expressions in Eq. (B15). Then along with the commutation and anticommutaion relations below, we substitute all of these in Eq. (8) to get the most general equation of motion for a single particle as shown below in Eq. (B18):

$$[\mathcal{H}, \rho] = i\omega(\hat{h} \times \vec{r}) \cdot \vec{\sigma},$$

$$\{\mathcal{H}, \rho\} = (\omega_0 + \omega r_e)\mathrm{I} + (\omega_0 \vec{r} + \omega \hat{h}) \cdot \vec{\sigma},$$

$$\{\ln(\rho), \rho\} = \frac{1}{2} \left[\ln \left(\frac{1-r^2}{4} \right) + r \ln \left(\frac{1+r}{1-r} \right) \right] \mathrm{I}$$
$$+ \frac{1}{2} \left[\ln \left(\frac{1-r^2}{4} \right) + \frac{1}{r} \ln \left(\frac{1+r}{1-r} \right) \right] \vec{r} \cdot \vec{\sigma}.$$

Using the commutation mentioned above and the trace relations, we find the (unscaled) β_i's to get the following expression (for the qubit case):

$$\beta_H = \frac{k r_e}{2\omega(1-r_e^2)} (\mathrm{A} - \mathrm{B}), \tag{B16}$$

$$\beta_I = \frac{k}{2\omega^2(1-r_e^2)} \left[\omega^2 (\mathrm{A} - r_e^2 \mathrm{B}) + \omega\omega_0 (\mathrm{A} - \mathrm{B}) \right], \tag{B17}$$

where $\mathrm{A} = [\ln(\frac{1-r^2}{4}) + r \ln(\frac{1+r}{1-r})]$ and $\mathrm{B} = [\ln(\frac{1-r^2}{4}) + \frac{1}{r} \ln(\frac{1+r}{1-r})]$. The equation of motion in this case is, with $\frac{d\rho}{dt} = \frac{1}{2} \frac{d\vec{r}}{dt} \cdot \vec{\sigma}$, and $r_e = 0$,

$$\frac{dr}{dt} = -\frac{1}{2\tau} (1-r^2) \ln \left(\frac{1+r}{1-r} \right). \tag{B18}$$

The solution to the above equation is Eq. (23). The form of Eq. (16) and in extension Eq. (20) is achieved by fixing the β_i's using required conditions in Eqs. (B16), and (B17). The above equations are strictly valid for $r < 1$ and in extension $|r_e| < 1$.

APPENDIX C: SOME COMMENTS ON τ

τ appears as a relaxation time associated with the system itself. As discussed in the literature [33,52,57,64] it is associated with the speed of evolution of the state operator. Considering a Fisher-Rao metric, which for probability space turns into a uniform metric, one can write from Eq. (A2) the following expression:

$$\frac{dl}{dt} = 2\sqrt{\dot{\gamma}_D \cdot \dot{\gamma}_D} = \dot{\epsilon}.$$

Here $\dot{\epsilon}$ is a small positive number, which fixes the norm of Π_γ and maximizes the direction as a consequence [52]. From the

evolution equation of state operator γ_D, we have

$$\dot{\gamma}_D = |\Pi_\gamma) = \frac{1}{\tau} \left| \Phi - \sum_i \beta_i \mathbf{C_i} \right).$$

Using these two and defining $|\Lambda)$ as an affinity vector that draws the motion towards SEA evolution, one can write the following expressions involving τ [52]:

$$\tau = \frac{\sqrt{(\Lambda \mid \Lambda)}}{\dot{\epsilon}}$$
$$= \frac{\left(\Phi - \sum_i \beta_i \mathbf{C_i} \mid \hat{G}^{-1} \mid \Phi - \sum_i \beta_i \mathbf{C_i} \right)}{\Pi_S}.$$

We see that τ is also inversely proportional to the entropy generation rate. As a result, for higher τ, we will see lesser entropy generation and lesser dissipation; as the speed is high, the system does not relax quickly. On the other hand, the system will relax faster, and entropy generation will be enhanced in case of low τ values. Both of these features of τ are explored in the main text. As can be seen, τ is dependent on ρ, yet as the literature suggests [33,52,57] constant nonzero τ can also work in elucidating the features of the general motion.

APPENDIX D: COMPUTATION OF β_i'S FOR THE QUANTUM WALKER

Considering, $\rho_u = \frac{1}{N}\mathrm{I}$, and $\mathcal{H}$ as given in Eq. (28), we begin by computing trace function as required in Eq. (B15), which are as given below:

$$\mathrm{tr}(\rho) = 1,$$
$$\mathrm{tr}(\rho\mathcal{H}) = d,$$
$$\mathrm{tr}(\rho\mathcal{H}^2) = N(d^2 + 2),$$
$$\mathrm{tr}[\rho \ln(\rho)] = -\ln(N),$$
$$\mathrm{tr}[\rho\mathcal{H} \ln(\rho)] = -d \ln(N).$$

Using these traces and noticing that Ω is given by

$$\mathrm{tr}(\rho\mathcal{H}^2)\mathrm{tr}(\rho) - [\mathrm{tr}(\rho\mathcal{H})]^2 = (N-1)d^2 + 2N,$$

we can write the expressions below for β_i's:

$$\begin{aligned} \beta_H &= 0, \\ \beta_I &= -\ln(N). \end{aligned} \tag{D1}$$

We have suppressed the t's for notational convenience.

---

[1] P. W. Shor, Polynomial-time algorithms for prime factorization and discrete logarithms on a quantum computer, SIAM Rev. **41**, 303 (1999).

[2] L. K. Grover, Quantum Mechanics Helps in Searching for a Needle in a Haystack, Phys. Rev. Lett. **79**, 325 (1997).

[3] Y. Aharonov, L. Davidovich, and N. Zagury, Quantum random walks, Phys. Rev. A **48**, 1687 (1993).

[4] A. M. Childs and J. Goldstone, Spatial search by quantum walk, Phys. Rev. A **70**, 022314 (2004).

[5] N. Shenvi, J. Kempe, and K. B. Whaley, Quantum random-walk search algorithm, Phys. Rev. A **67**, 052307 (2003).

[6] E. Farhi and S. Gutmann, Analog analogue of a digital quantum computation, Phys. Rev. A **57**, 2403 (1998).

[7] K. Manouchehri and J. B. Wang, Continuous-time quantum random walks require discrete space, J. Phys. A: Math. Theor. **40**, 13773 (2007).

[8] A. M. Childs, Universal Computation by Quantum Walk, Phys. Rev. Lett. **102**, 180501 (2009).

[9] T. A. Brun, H. A. Carteret, and A. Ambainis, Quantum walks driven by many coins, Phys. Rev. A **67**, 052317 (2003).

[10] A. Nayak and A. Vishwanath, Quantum walk on the line, arXiv:quant-ph/0010117 (2000).

[11] Y. Omar, N. Paunković, L. Sheridan, and S. Bose, Quantum walk on a line with two entangled particles, Phys. Rev. A **74**, 042304 (2006).

[12] P. K. Pathak and G. S. Agarwal, Quantum random walk of two photons in separable and entangled states, Phys. Rev. A **75**, 032351 (2007).

[13] K. Manouchehri and J. Wang, *Physical Implementation of Quantum Walks* (Springer, Berlin, 2014).

[14] V. Kendon, Decoherence in quantum walks—A review, Math. Struct. Comput. Sci. **17**, 1169 (2007).

[15] L. E. Fedichkin and F. P. Meshchaninov, Analysis and applications of quantum walks, J. Math. Sci. **252**, 104 (2021).

[16] A. M. Childs, On the relationship between continuous- and discrete-time quantum walk, Commun. Math. Phys. **294**, 581 (2010).

[17] D. D'Alessandro, Connection between continuous and discrete time quantum walks. From *D*-dimensional lattices to general graphs, Rep. Math. Phys. **66**, 85 (2010).

[18] F. W. Strauch, Connecting the discrete- and continuous-time quantum walks, Phys. Rev. A **74**, 030301 (2006).

[19] D. Aharonov, A. Ambainis, J. Kempe, and U. Vazirani, Quantum walks on graphs, in *Proceedings of the Thirty-Third Annual ACM Symposium on Theory of Computing, Hersonissos, Greece* (Association for Computing Machinery, New York, NY, 2001), pp. 50–59.

[20] P. P. Rohde, A. Schreiber, M. Štefaňák, I. Jex, and C. Silberhorn, Multi-walker discrete time quantum walks on arbitrary graphs, their properties and their photonic implementation, New J. Phys. **13**, 013001 (2011).

[21] P. P. Rohde, A. Fedrizzi, and T. C. Ralph, Entanglement dynamics and quasi-periodicity in discrete quantum walks, J. Mod. Opt. **59**, 710 (2012).

[22] A. Romanelli, Distribution of chirality in the quantum walk: Markov process and entanglement, Phys. Rev. A **81**, 062349 (2010).

[23] A. Romanelli, Thermodynamic behavior of the quantum walk, Phys. Rev. A **85**, 012319 (2012).

[24] A. Romanelli, R. Donangelo, R. Portugal, and F. de Lima Marquezino, Thermodynamics of *n*-dimensional quantum walks, Phys. Rev. A **90**, 022329 (2014).

[25] V. Kendon and B. Tregenna, Decoherence can be useful in quantum walks, Phys. Rev. A **67**, 042315 (2003).

[26] L. Fedichkin, D. Solenov, and C. Tamon, Mixing and decoherence in continuous-time quantum walks on cycles, arXiv:quant-ph/0509163 (2005).

[27] M. A. Nielsen and I. L. Chuang, *Quantum Computation and Quantum Information* (Cambridge University Press, Cambridge, 2000).

[28] S. Chakraborty, K. Luh, and J. Roland, How Fast Do Quantum Walks Mix? Phys. Rev. Lett. **124**, 050501 (2020).

[29] S. Chakraborty, K. Luh, and J. Roland, Analog quantum algorithms for the mixing of Markov chains, Phys. Rev. A **102**, 022423 (2020).

[30] J. D. Whitfield, C. A. Rodríguez-Rosario, and A. Aspuru-Guzik, Quantum stochastic walks: A generalization of classical random walks and quantum walks, Phys. Rev. A **81**, 022323 (2010).

[31] S. Garnerone, Thermodynamic formalism for dissipative quantum walks, Phys. Rev. A **86**, 032342 (2012).

[32] A. Candeloro, L. Razzoli, S. Cavazzoni, P. Bordone, and M. G. A. Paris, Continuous-time quantum walks in the presence of a quadratic perturbation, Phys. Rev. A **102**, 042214 (2020).

[33] G. Li and M. R. von Spakovsky, Generalized thermodynamic relations for a system experiencing heat and mass diffusion in the far-from-equilibrium realm based on steepest entropy ascent, Phys. Rev. E **94**, 032117 (2016).

[34] M. Grmela and H. C. Öttinger, Dynamics and thermodynamics of complex fluids. I. Development of a general formalism, Phys. Rev. E **56**, 6620 (1997).

[35] H. C. Öttinger and M. Grmela, Dynamics and thermodynamics of complex fluids. II. Illustrations of a general formalism, Phys. Rev. E **56**, 6633 (1997).

[36] G. P. Beretta, Maximum entropy production rate in quantum thermodynamics, J. Phys.: Conf. Ser. **237**, 012004 (2010).

[37] G. P. Beretta, A theorem on Lyapunov stability for dynamical systems and a conjecture on a property of entropy, J. Math. Phys. **27**, 305 (1986).

[38] G. N. Hatsopoulos and E. P. Gyftopoulos, A unified quantum theory of mechanics and thermodynamics. Part I. Postulates, Found. Phys. **6**, 15 (1976).

[39] G. N. Hatsopoulos and E. P. Gyftopoulos, A unified quantum theory of mechanics and thermodynamics. Part IIa. Available energy, Found. Phys. **6**, 127 (1976).

[40] G. N. Hatsopoulos and E. P. Gyftopoulos, A unified quantum theory of mechanics and thermodynamics. Part IIb. Stable equilibrium states, Found. Phys. **6**, 439 (1976).

[41] G. N. Hatsopoulos and E. P. Gyftopoulos, A unified quantum theory of mechanics and thermodynamics. Part III. Irreducible quantal dispersions, Found. Phys. **6**, 561 (1976).

[42] G. P. Beretta, E. P. Gyftopoulos, J. L. Park, and G. N. Hatsopoulos, Quantum thermodynamics. A new equation of motion for a single constituent of matter, Nuovo Cimento B (1971–1996) **82**, 169 (1984).

[43] G. P. Beretta, Entropy and irreversibility for a single isolated two level system: New individual quantum states and new nonlinear equation of motion, Int. J. Theor. Phys. **24**, 119 (1985).

[44] G. P. Beretta, E. P. Gyftopoulos, and J. L. Park, Quantum thermodynamics. A new equation of motion for a general quantum system, Nuovo Cimento B (1971–1996) **87**, 77 (1985).

[45] G. P. Beretta, Steepest entropy ascent in quantum thermodynamics, in *The Physics of Phase Space Nonlinear Dynamics and Chaos Geometric Quantization, and Wigner Function*, edited by Y. S. Kim and W. W. Zachary (Berlin, Heidelberg, 1987), pp. 441–443.

[46] S. Gheorghiu-Svirschevski, Nonlinear quantum evolution with maximal entropy production, Phys. Rev. A **63**, 022105 (2001).

[47] S. Gheorghiu-Svirschevski, Addendum to "Nonlinear quantum evolution with maximal entropy production," Phys. Rev. A **63**, 054102 (2001).

[48] S. Cano-Andrade, G. P. Beretta, and M. R. von Spakovsky, Steepest-entropy-ascent quantum thermodynamic modeling of decoherence in two different microscopic composite systems, Phys. Rev. A **91**, 013848 (2015).

[49] G. P. Beretta, The fourth law of thermodynamics: Steepest entropy ascent, Philos. Trans. R. Soc. A **378**, 20190168 (2020).

[50] P. Ván, Nonequilibrium thermodynamics: Emergent and fundamental, Philos. Trans. R. Soc. A **378**, 20200066 (2020).

[51] G. P. Beretta, Nonlinear extensions of Schrödinger–von Neumann quantum dynamics: A set of necessary conditions for compatibility with thermodynamics, Mod. Phys. Lett. A **20**, 977 (2005).

[52] G. P. Beretta, Steepest entropy ascent model for far-nonequilibrium thermodynamics: Unified implementation of the maximum entropy production principle, Phys. Rev. E **90**, 042113 (2014).

[53] A. Montefusco, F. Consonni, and G. P. Beretta, Essential equivalence of the general equation for the nonequilibrium reversible-irreversible coupling (generic) and steepest-entropy-ascent models of dissipation for nonequilibrium thermodynamics, Phys. Rev. E **91**, 042138 (2015).

[54] G. Li and M. R. von Spakovsky, Steepest-entropy-ascent quantum thermodynamic modeling of the relaxation process of isolated chemically reactive systems using density of states and the concept of hypoequilibrium state, Phys. Rev. E **93**, 012137 (2016).

[55] I. Kim and M. R. von Spakovsky, *Ab initio* relaxation times and time-dependent Hamiltonians within the steepest-entropy-ascent quantum thermodynamic framework, Phys. Rev. E **96**, 022129 (2017).

[56] E. Farhi and S. Gutmann, Quantum computation and decision trees, Phys. Rev. A **58**, 915 (1998).

[57] G. P. Beretta, Nonlinear quantum evolution equations to model irreversible adiabatic relaxation with maximal entropy production and other nonunitary processes, Rep. Math. Phys. **64**, 139 (2009).

[58] A. Vallejo, A. Romanelli, and R. Donangelo, Qubit thermodynamics far from equilibrium: Two perspectives about the nature of heat and work in the quantum regime, Phys. Rev. E **103**, 042105 (2021).

[59] J. L. Park and W. Band, A general theory of empirical state determination in quantum physics: Part I, Found. Phys. **1**, 211 (1971).

[60] W. Band and J. L. Park, A general method of empirical state determination in quantum physics: Part II, Found. Phys. **1**, 339 (1971).

[61] G. Kimura, The Bloch vector for N-level systems, Phys. Lett. A **314**, 339 (2003).

[62] R. A. Bertlmann and P. Krammer, Bloch vectors for qudits, J. Phys. A: Math. Theor. **41**, 235303 (2008).

[63] M. Ozols and L. Mancinska, Generalized Bloch vector and the eigenvalues of a density matrix, http://home.lu.lv/~sd20008/papers/Bloch%20Vectors%20and%20Eigenvalues.pdf (2020).

[64] G. Li, M. R. von Spakovsky, and C. Hin, Steepest entropy ascent quantum thermodynamic model of electron and phonon transport, Phys. Rev. B **97**, 024308 (2018).